PRDW
Consulting Port and Coastal Engineers

GRANGER BAY EXECUTION PHASE

Wave Modelling Report

Detail Design

GB00-PRD-XX-XX-RP-MA-0002

27 January 2025

V&A WATERFRONT
Cape Town, South Africa

V&A WATERFRONT · CAPE TOWN ·

PRDW
Consulting Port and Coastal Engineers

GRANGER BAY EXECUTION PHASE

Wave Modelling Report

Detail Design

GB00-PRD-XX-XX-MA-0002

27 January 2025

REVISION	DATE	EXECUTED	CHECK	APPROVED	CLIENT	DESCRIPTION / COMMENTS
A	27-01-2025	SRW	SAL			Draft

(A) Interdisciplinary coordination (B) For approval (C,D,E…) Modifications (0) Approved (1,2,3…) Scope modification (N) Void

Management System ISO 9001:2015 TÜVRheinland CERTIFIED www.tuv.com ID 9105074573

SABS ISO 9001

V&A WATERFRONT
Cape Town, South Africa

V&A WATERFRONT · CAPE TOWN ·

PRDW
Consulting Port and Coastal Engineers

CONTENT

PRDW
Consulting Port and Coastal Engineers

TABLES

FIGURES

V&A WATERFRONT

GRANGER BAY EXECUTION PHASE

Wave Modelling Report

1. INTRODUCTION

1.1 Background

PRDW have been appointed by the V&A Waterfront for the design of the marine infrastructure required for the Granger Bay development, located between the Western dolos revetment and the Granger Bay Small Craft Harbour, also known as the Waterclub. The location of the development area is presented in Figure 1-1.

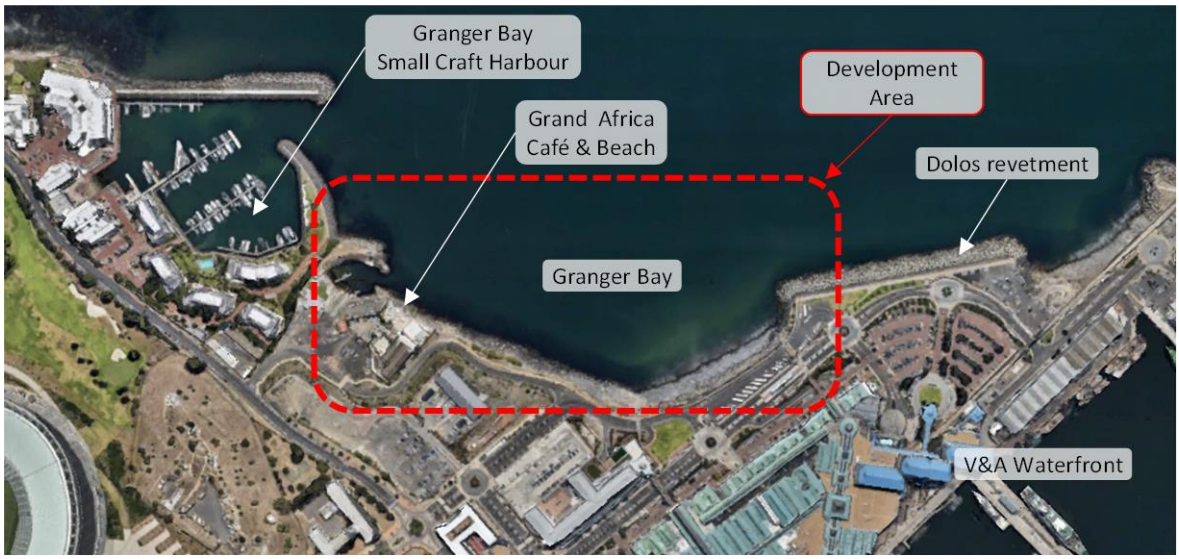

Figure 1-1: Site location.

Layout Option 1, as shown in Figure 1-2 was agreed between Heatherwick, V&A and PRDW as the preferred solution, provided it fitted within the budget. Preliminary cost estimates indicated that this layout is within budget and therefore it has been carried forward to the physical modelling stage to further investigate its viability and performance.

Figure 1-2: Heatherwick layout of Granger Bay carried forward to detailed design and model testing.

PRDW have been appointed to undertake a numerical modelling study of the proposed development, with the aim of developing extreme wave conditions for the design and providing input into the physical modelling. This report describes the numerical wave model results for the layout shown in Figure 1-2, whilst the modelling for previous versions of the development layout are described in (PRDW, 2022).

1.2 Terms of reference

The terms of reference for this numerical wave modelling study are to produce the following main outputs:

- Extreme wave conditions along the edges of the proposed development to provide input into the design and the physical modelling.
- Wave run-up and overtopping of edge structures during extreme events to provide input into the design.

1.3 Scope of work

The scope of work for the wave modelling included the following:

- Spectral wave modelling to determine the nearshore extreme wave conditions.
- Wave penetration and overtopping modelling to assess the wave conditions in and around the proposed development and to assess the overtopping of the edge structures.

The scope includes the baseline layout (no development) and the development layout shown in Figure 1-2, defined by a plan layout and cross-sections defining crest levels, slope and armour.

1.4 Report structure

Section 2 describes the climate change considerations for the increase in sea level, extreme wave height and storm surge. Section 3 contains the tide and storm surge analysis on measured water levels at Cape Town.

The spectral wave modelling is described in Section 4. Section 5 presents the wave penetration and overtopping modelling and results. A summary of the study is presented in Section 6.

1.5 Datum and coordinate reference system

The vertical datum adopted in this study is mean sea level (MSL), which is 0.825 m above Chart Datum (CD).

The WG19 horizontal coordinate system was used for this study. All spatial plots include x and y axes showing the x and y coordinates in meters in the WG19 system. True north is always pointing upwards.

2. CLIMATE CHANGE

2.1 Basis

The effect of Climate Change on the design parameters over the design life of the development was included in the study. Based on an estimated construction date of 2024 and a design life of 50 years, projections have been derived for the following time horizons:

- 2024 (end of construction)
- 2074 (end of design life)

The projections are based on the latest information available from the 6th Assessment Report: Physical Science Basis (IPCC, In press) of the Intergovernmental Panel for Climate Change (IPCC) and supplemented with other relevant literature.

The AR6 presents projections for a range of emissions scenarios, referred to as Shared Socioeconomic Pathways (SSPs). This is an update of the Representative Concentration Pathways (RCPs) used in the 5th Assessment Report. In this study, median projections for the most conservative scenario (SSP5-8.5) have been used. Where projections are not yet available for SSP5-8.5, the nominally corresponding scenario from AR5 was used (RCP8.5).

2.2 Sea level rise

Projections for sea level rise (SLR) were based on the latest projections provided in AR6, which can be downloaded from the NASA Sea Level Change Portal (https://sealevel.nasa.gov/). Figure 2-1 presents the regional relative SLR at Cape Town for the median and upper end of the likely range for SSP5-8.5. The projections are referred to as relative since they include an estimate of long-term vertical land motion to provide projections relative to the land. While the IPCC projections are given relative to a baseline period of 1995-2014, the curves shown in the figure are presented relative to 2019, the baseline date for Mean Level at Cape Town (see Section 3.1).

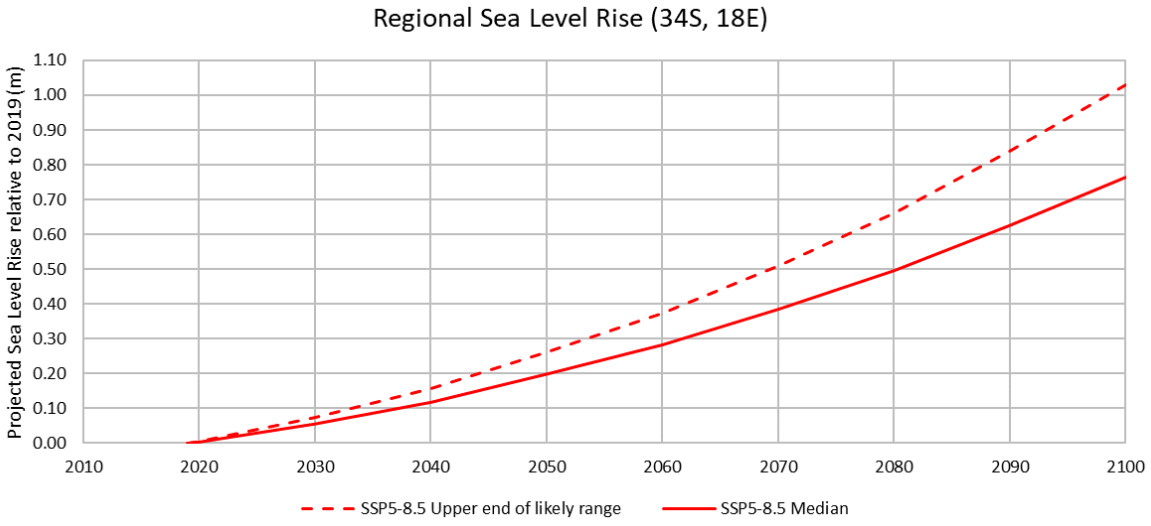

Figure 2-1: Regional relative sea level rise at Cape Town from AR6 (IPCC, In press), showing the median and upper end of the likely range for SSP5-8.5. Baseline date is 2019.

The median projections for SSP5-8.5 were used in this study and are presented in Table 2-1.

2.3 Storm surge

Storm surge is mainly composed of an atmospheric pressure component (low pressure for positive storm surge and high pressure for a negative storm surge) and a wind-induced component. The atmospheric pressure component of storm surge is proportional to the gradient in atmospheric pressure through the inverse barometer effect, while the wind setup component of storm surge is proportional to the square of the wind speed.

Projections of wind speed and extreme sea level pressure were obtained from a 50 km resolution downscaled climate model ensemble run by the Council for Scientific and Industrial Research, as described in Airshed (2021) The data includes timeseries of spatially averaged meteorological parameters over an area of 100 km by 100 km at Cape Town for a period of 1960-2099 and provides projections for RCP8.5. The data included the annual maximum hourly wind speed and annual mean sea level pressure. In lieu of data on extreme sea level pressure, the projected percentage change for extreme low pressure was assumed the same as for the annual mean.

The projected increases in extreme wind speed were larger than the projected decreases in mean sea level pressure. In lieu of detailed projections available in literature, the projections for storm surge used here were based on the conservative assumption that the wind setup component is dominant and were thus determined as the square of the projected extreme wind speed increase. The resulting projections applied in the study are presented in Table 2-1.

2.4 Extreme wave height

Projections for global changes in extreme wave heights have been determined from a seven-member wave model ensemble (Meucci, Young, Hemer, Ranashinge, & Kirezci, 2020). For each of a present-day (1979-2005) and future time slice (2081-2100), extreme wave heights were determined by fitting an exponential distribution to the 1 000 highest wave heights pooled from the seven models (after bias-correction). The projected changes for the 100-year return period significant wave height (H_{m0}) were linearly interpolated to the required dates, and converted to a baseline date of 2000, the mid-point of the dataset used to derive the extreme wave climate (see Section 4.6). The resulting projections applied in the study are presented in Table 2-1.

2.5 Summary

The Climate Change projections used in this study are summarised in Table 2-1.

Table 2-1: Climate Change applied for each parameter and date.

Parameter	Description	Scenario	Units	Baseline date	2024	2074
Sea level rise (SLR)	Regional relative mean sea level rise	SSP5-8.5 (median)	m	2019	0.02	0.43
Wind speed	Annual maximum hourly averaged wind speed	RCP8.5 (mean)	%	1993.5	0.6%	2.0%
Storm surge	Extreme positive	RCP8.5 (mean)	%	1993.5	1.2%	4.0%
Wave height	Extreme wave height in deep water offshore	RCP8.5, no uncertainty ranges available	%	2000	0.9%	2.8%

3. WATER LEVEL ANALYSIS

3.1 Measured water levels

The hourly measured water levels for Cape Town for the period 1967 to 2020 were analysed for this study. The tide gauge was initially located in Granger Bay and was later moved to the North Spur within the Port of Cape Town. The hourly measured data are plotted in Figure 3-1.

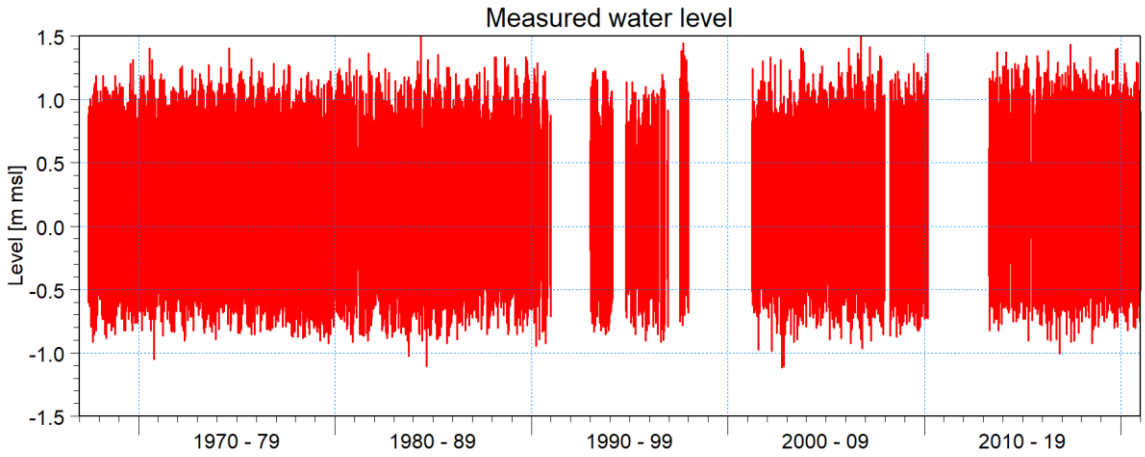

Figure 3-1: Measured hourly water levels at Cape Town.

A linear regression fitted to the annual average water level over the measured period indicated a trend of +0.94 mm/year, which was removed prior to further analysis. Tidal harmonic analyses were carried out using the MIKE 21 tidal analysis and prediction toolbox (DHI, 2024a) to obtain the tidal constituents for the detrended Cape Town datasets.

The constituents were used to generate the predicted tide. The Mean Level (ML) of +0.20 m MSL was calculated as the arithmetic average of the monthly mean levels over a recent measurement period (2018 to 2020) which had good data coverage. The level is representative of a baseline date of 2019, the approximate mid-point of the dataset. The resulting predicted tidal levels for Cape Town are presented in Table 3-1. Figure 3-2 presents the percentiles of the high tides of the predicted tide over a continuous 19-year period.

Table 3-1: Predicted tidal levels for Cape Town (2019 base date).

Tidal heights	Tidal level [m MSL]
Highest Astronomical Tide (HAT)	1.255
Mean High Water Spring (MHWS)	0.950
Mean High Water Neap (MHWN)	0.462
Mean Level (ML)	0.201
Mean Low Water Neap (MLWN)	-0.058
Mean Low Water Spring (MLWS)	-0.526
Lowest Astronomical Tide (LAT)	-0.766

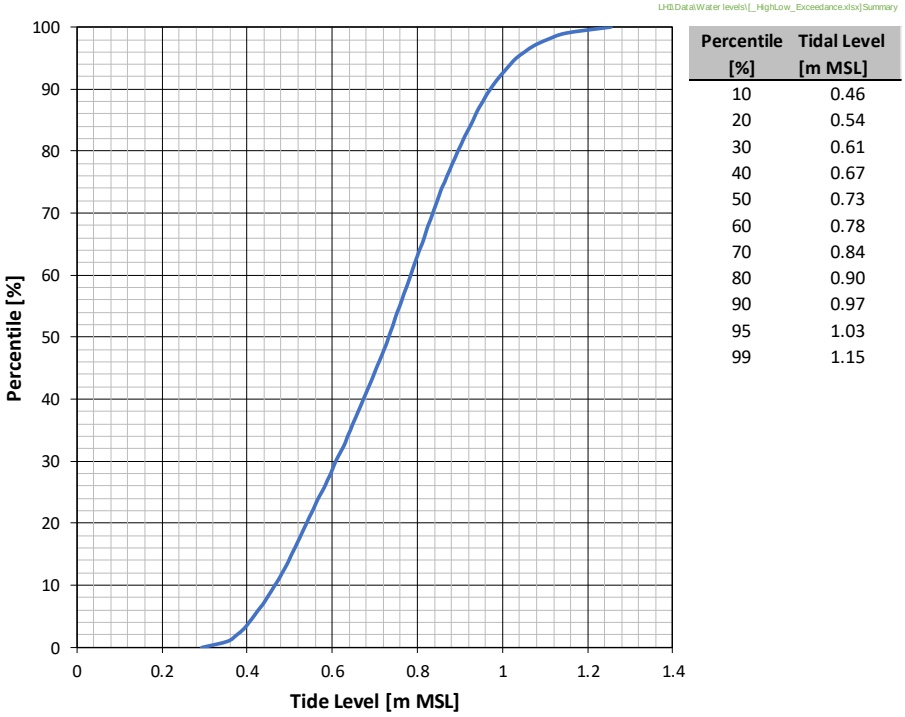

Figure 3-2: Percentiles of the predicted high tides over a continuous 19-year period.

The 90th percentile high tide (+0.97 m MSL) was selected as the initial tidal water level to apply for the extreme wave model runs. This is defined as the high tide level that is exceeded by 10 percent of the high tides over a continuous 19-year period, as shown in Figure 3-2. The 90th percentile high tide is similar in height to MWHS at Cape Town (+0.95 m MSL) but has the advantage that the exceedance thereof is quantified (i.e., 10% of the high tides are higher).

3.2 Storm surge

The predicted tide in the Port of Cape Town was subtracted from the detrended measured water level (Section 3.1) to obtain the storm surge. The measured water level, predicted tide and storm surge are plotted in Figure 3-3.

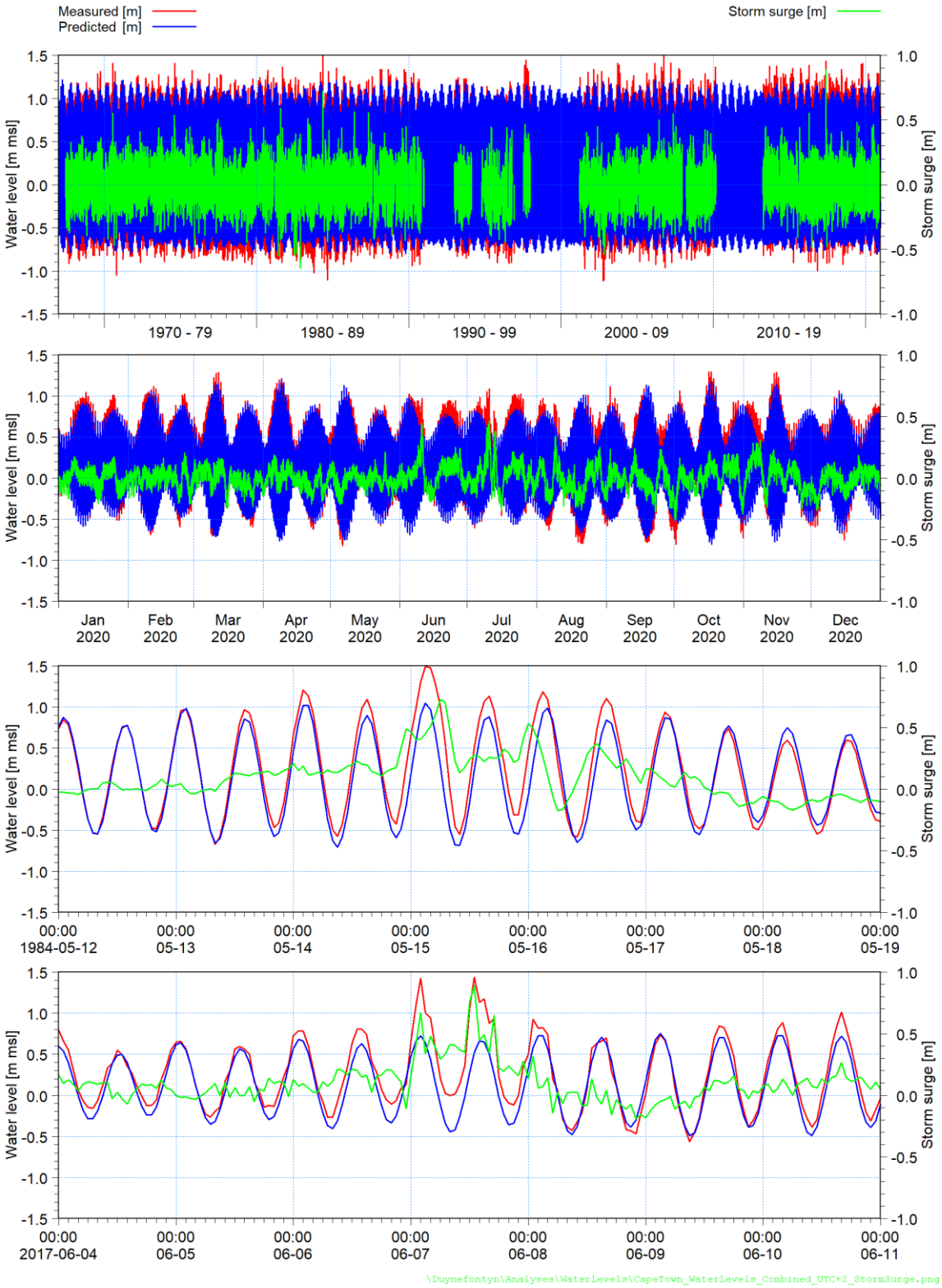

Figure 3-3: Measured water level, predicted tide and storm surge at Cape Town for the entire dataset (top), detail for 2020 (top middle), the May 1984 storm (bottom middle) and the June 2017 storm (bottom).

An extreme value analysis (EVA) was performed on the positive storm surge (measured water level higher than predicted tide) using the 'MIKE by DHI' EVA toolbox (DHI, 2024b). The analysis comprises fitting a three parameter Weibull distribution using the Method of Moments to an extreme value series extracted from the

input timeseries. The extreme value series was selected using the 'peaks over threshold' or 'partial duration series' method, with the threshold defined as the value that is exceeded four times per year on average. To ensure independence, two successive events were extracted only if the time between the events exceeded 48 hours. The uncertainty was calculated using Jack knife resampling to evaluate the mean and standard deviation of the estimate to obtain the upper 95% confidence (97.5th percentile) estimates.

The extreme value analysis results for positive storm surge are plotted in Figure 3-4. The EVA was used to determine the extreme storm surge for the 1, 10, 47.5, 100, and 475-year return periods.

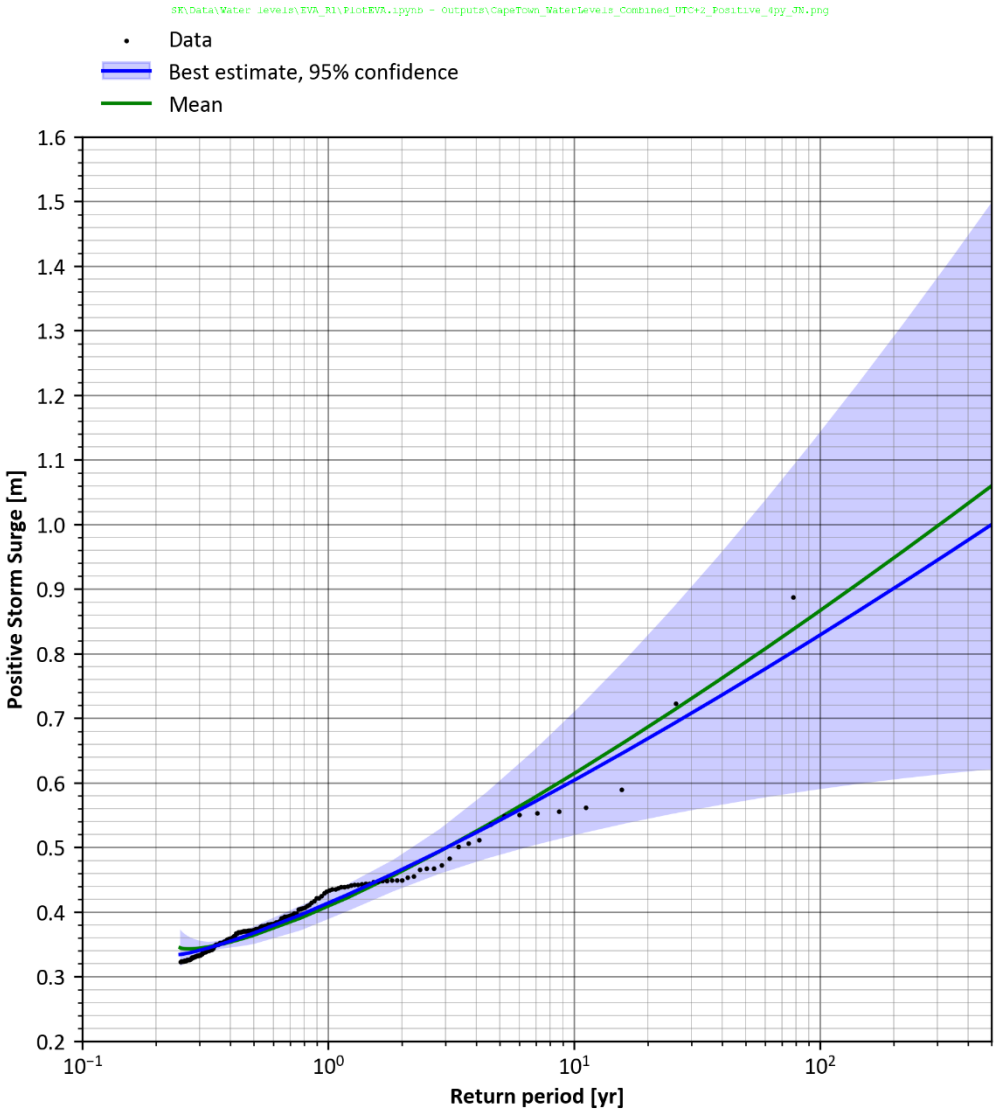

Figure 3-4: Extreme value analysis of positive storm surge residuals at Cape Town (baseline date is 1993.5).

The above analysis was based on an extreme value series of four events per year on average. This allows accurate characterisation of extreme events (e.g. 1-year and above), but does not allow characterisation of lower return periods. Based on the joint probability between waves and storm surge (see Section 4.6.2), this study also required an estimate of the 0.1-year storm surge. This was obtained from a second EVA of the same data but based on selecting ten events per year on average. The extreme storm surge combined from both analyses is summarised in Table 3-2.

Table 3-2: Extreme positive storm surge from the extreme value analyses.

Return period [y]	Uncertainty	Positive storm surge [m]
0.1	Lower 95% confidence limit	0.25
	Best estimate	0.27
	Upper 95% confidence limit	0.29
1	Lower 95% confidence limit	0.39
	Best estimate	0.41
	Upper 95% confidence limit	0.43
10	Lower 95% confidence limit	0.52
	Best estimate	0.60
	Upper 95% confidence limit	0.71
47.5	Lower 95% confidence limit	0.57
	Best estimate	0.75
	Upper 95% confidence limit	0.99
100	Lower 95% confidence limit	0.59
	Best estimate	0.83
	Upper 95% confidence limit	1.14
475	Lower 95% confidence limit	0.62
	Best estimate	0.99
	Upper 95% confidence limit	1.49

The baseline date is 1993.5 which is the middle of the measurement period. The best estimate positive storm surge was adjusted for Climate Change (refer to Table 2-1) and added to the 90th percentile high tide and the sea level rise to obtain the maximum still water level at the two dates of interest. Table 3-3 summarises the adjusted still water levels due to Climate Change.

Table 3-3: Best estimate extreme still water levels.

Return period [y]	Tide[(a)] [m MSL]	Sea level rise[(b)] [m]		Positive storm surge[(c)] [m]		Still water level[(d)] [m MSL]	
		2024	2074	2024	2074	2024	2074
0.1	0.97	0.02	0.43	0.27	0.28	1.26	1.68
1	0.97	0.02	0.43	0.41	0.43	1.40	1.83
10	0.97	0.02	0.43	0.61	0.62	1.60	2.02
47.5	0.97	0.02	0.43	0.76	0.78	1.75	2.18
100	0.97	0.02	0.43	0.84	0.86	1.83	2.26
475	0.97	0.02	0.43	1.00	1.03	1.99	2.43

(a) 90th percentile high tide
(b) Baseline date is 2019. Refer to Table 2-1 for Climate Change projections.
(c) Best estimate storm surge, adjusted for climate change (baseline date is 1993.5)
(d) Still water level is the sum of the tide, sea level rise and positive storm surge. Still water level excludes wave effects.

4. SPECTRAL WAVE MODELLING

4.1 Model description

The MIKE 21 Spectral Waves (SW) Flexible Mesh model was used to provide nearshore extreme wave conditions at Granger Bay as required for input to the wave penetration and overtopping modelling described in Section 5.

The application of the model is described in the User Manual (DHI, 2024c), while full details of the physical processes being simulated and the numerical solution techniques are described in the Scientific Documentation (DHI, 2024d). The model simulates the growth, decay and transformation of wind-generated waves and swells in offshore and coastal areas using unstructured meshes.

The model was run using the instationary time formulation with the fully spectral formulation, including the following physical phenomena:

- Wind-wave generation;
- Non-linear wave-wave interaction;
- Dissipation due to whitecapping;
- Dissipation due to bottom friction;
- Dissipation due to depth-induced wave breaking;
- Refraction and shoaling due to depth variations; and
- The effect of time-varying water depth.

4.2 Mesh and bathymetry

The model mesh comprises triangles with a resolution varying from about 11 km at the offshore boundary to about 160 m nearshore.

The model bathymetry has been obtained from the following sources:

- CMAP electronic hydrographic charts (DHI, 2024e),
- Available bathymetric surveys in Table Bay,
- Granger Bay hydrographic survey (Underwater Surveys, 2022).

Figure 4-1 and Figure 4-2 show the model bathymetry and mesh, respectively, and the location of an Acoustic Doppler Current Profiler (ADCP) moored at position (X = -56 401 m, Y = -3 751 487 m, depth = -25.8 m MSL) previously used for calibration of the wave model.

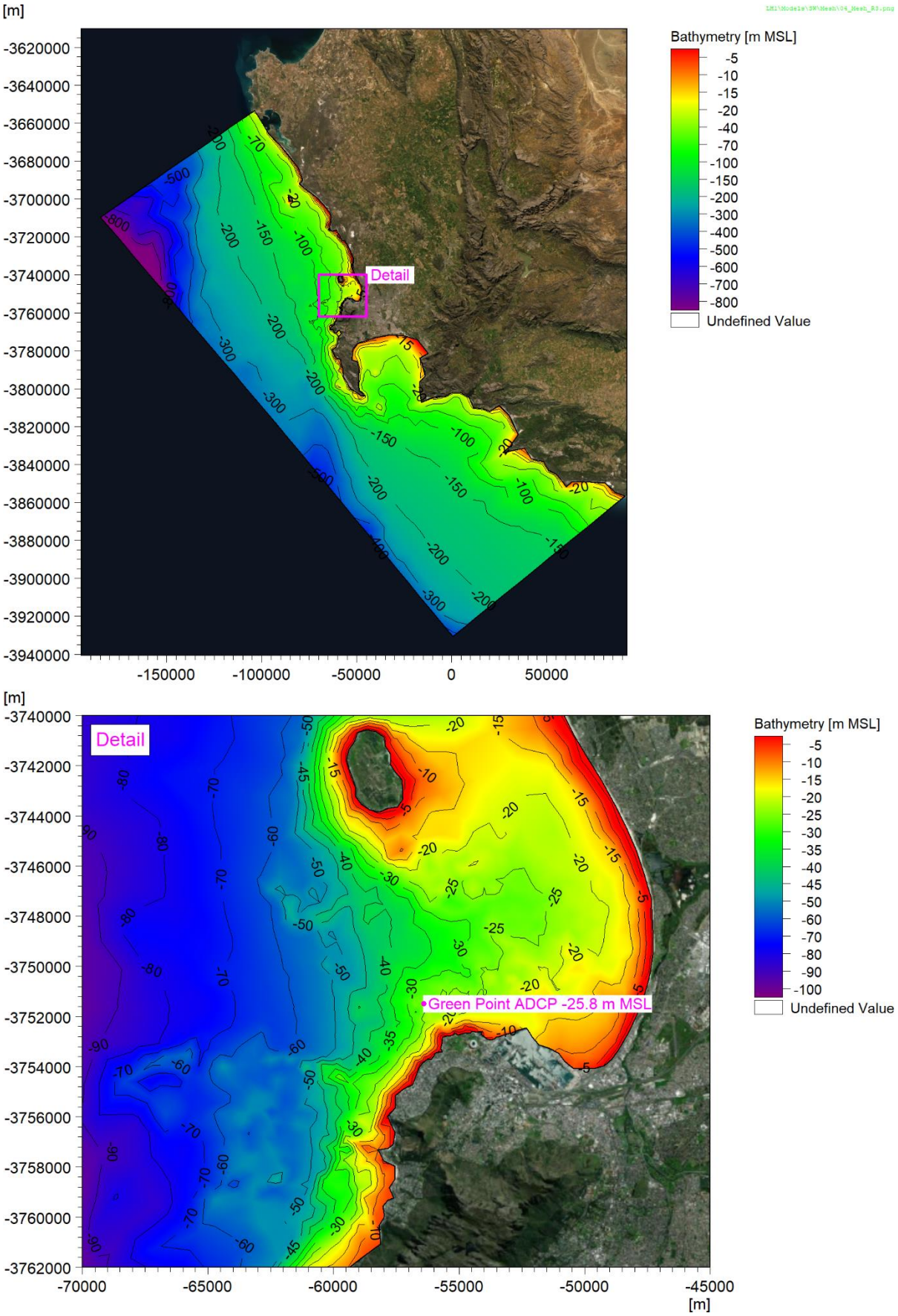

Figure 4-1: Model bathymetry.

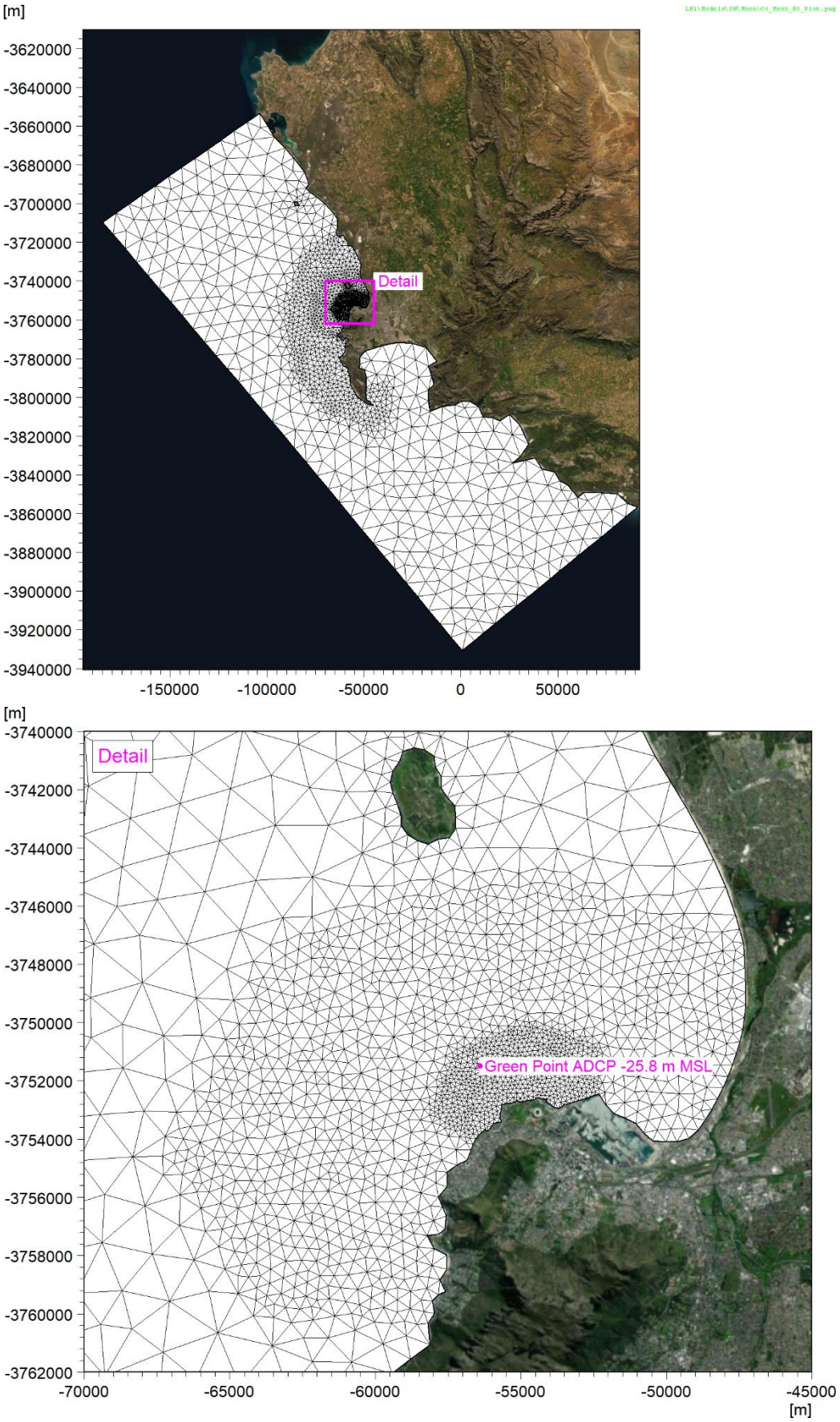

Figure 4-2: Model mesh.

4.3 Boundary conditions

Hindcast wave data was obtained from the NOAA/NCEP WAVEWATCH III CFSR Hindcast Dataset (NCEP, 2022). Three datasets are currently available namely the Reanalysis (1979-2009), Production (2005-2019) and Forecast (2007-2021). The Reanalysis and Production datasets contain fully spectral wave data at one-hourly intervals, available in deep water at 1 degree intervals on a longitude/latitude grid. The Forecast dataset is available at 0.5 degree intervals at 3-hourly intervals. The order of preference for the datasets was Reanalysis, Production, then Forecast. The hindcast spectral wave data was applied along the north-western to south-eastern boundary with lateral wave boundaries connecting the land and the spectral boundaries at the northern and eastern extents.

In addition to the wave forcing, the NCEP datasets also include space and time varying 10 m wind fields. This was applied as a space and time-varying wind field over the model domain. The uncoupled formulation of air-sea interaction was used for the wind-wave generation.

Bottom friction was modelled using a spatially varying Nikuradse roughness ranging between k_N = 0.02 m and 0.10 m, based on the seabed type. The predicted tidal levels at Cape Town (Section 3.1) were applied as a time-varying, space constant water level.

4.4 Calibration to nearshore measurements

The model has previously been calibrated to wave data measured at Green Point in -25.8 m MSL, as shown in Figure 4-1. Fully spectral waves at hourly intervals were measured during two periods, namely a six-week winter/spring period with measurements between 21 August 2019 and 3 October 2019, and a 10-week summer/autumn period with measurements between 13 February 2020 and 23 April 2020.

A wave refraction plot for a west-south-westerly wave event is shown in Figure 4-3.

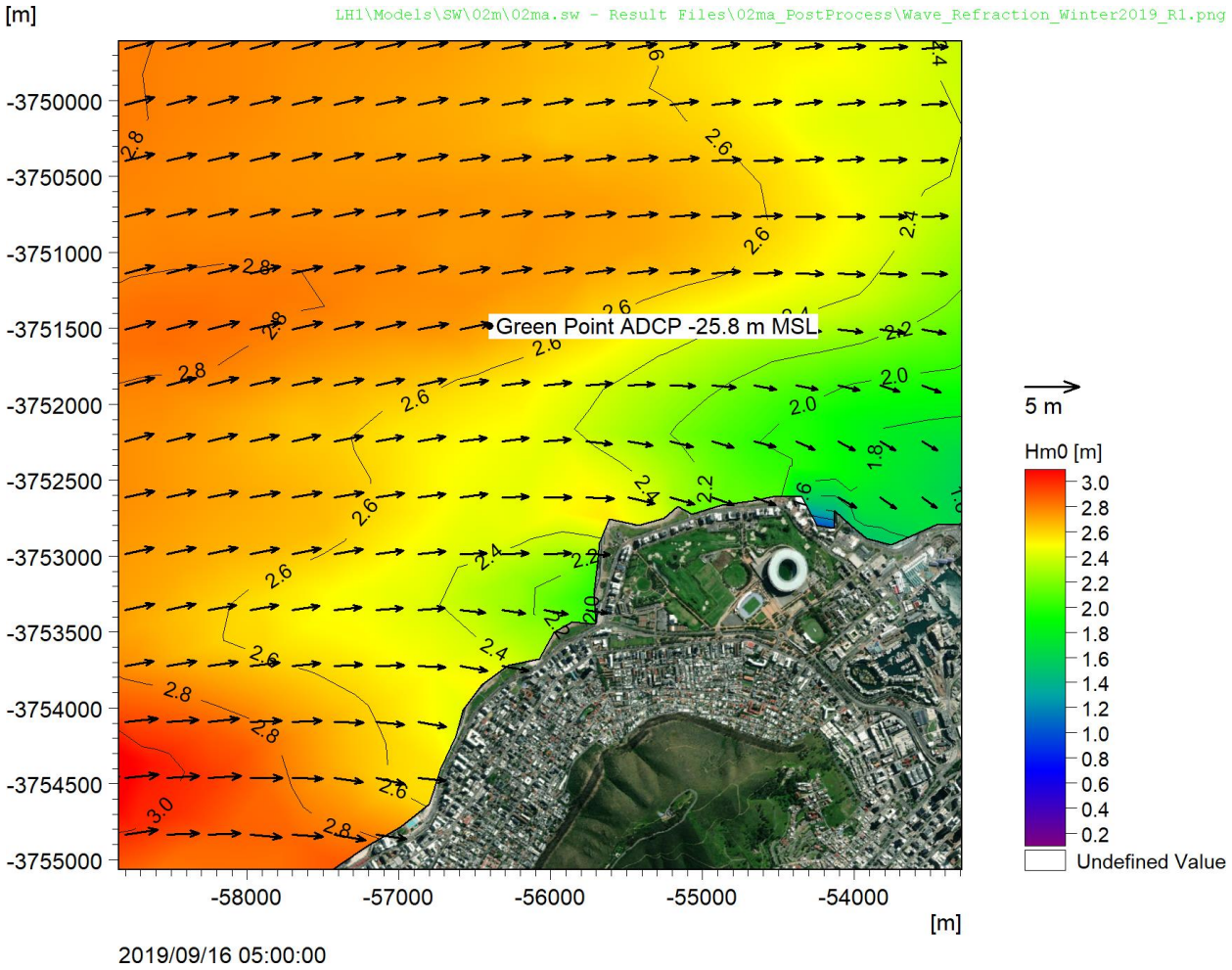

Figure 4-3: Wave refraction plot for a west-south-westerly wave event. The wave condition at the offshore boundary is H_{m0} = 3.24 m, T_P = 13.4 s, D_{MP} = 257.5°.

Figure 4-4 and Figure 4-5 present a timeseries comparison of measured and modelled significant wave height (H_{m0}), peak wave period (T_P) and mean wave direction at T_P (D_{MP}) at the ADCP for the Winter/Spring 2019 and Summer/Autumn 2020 periods respectively. The significant wave height percentile plots are shown in Figure 4-6 and Figure 4-7 to compare the measured and modelled wave heights. Measured and modelled wave roses are shown in Figure 4-8 and Figure 4-9 for both measurement periods. A scatter graph showing the measured versus modelled H_{m0} for both measurement periods combined is shown in Figure 4-10. By convention, wave direction is the direction from which the wave is coming, measured clockwise from true north.

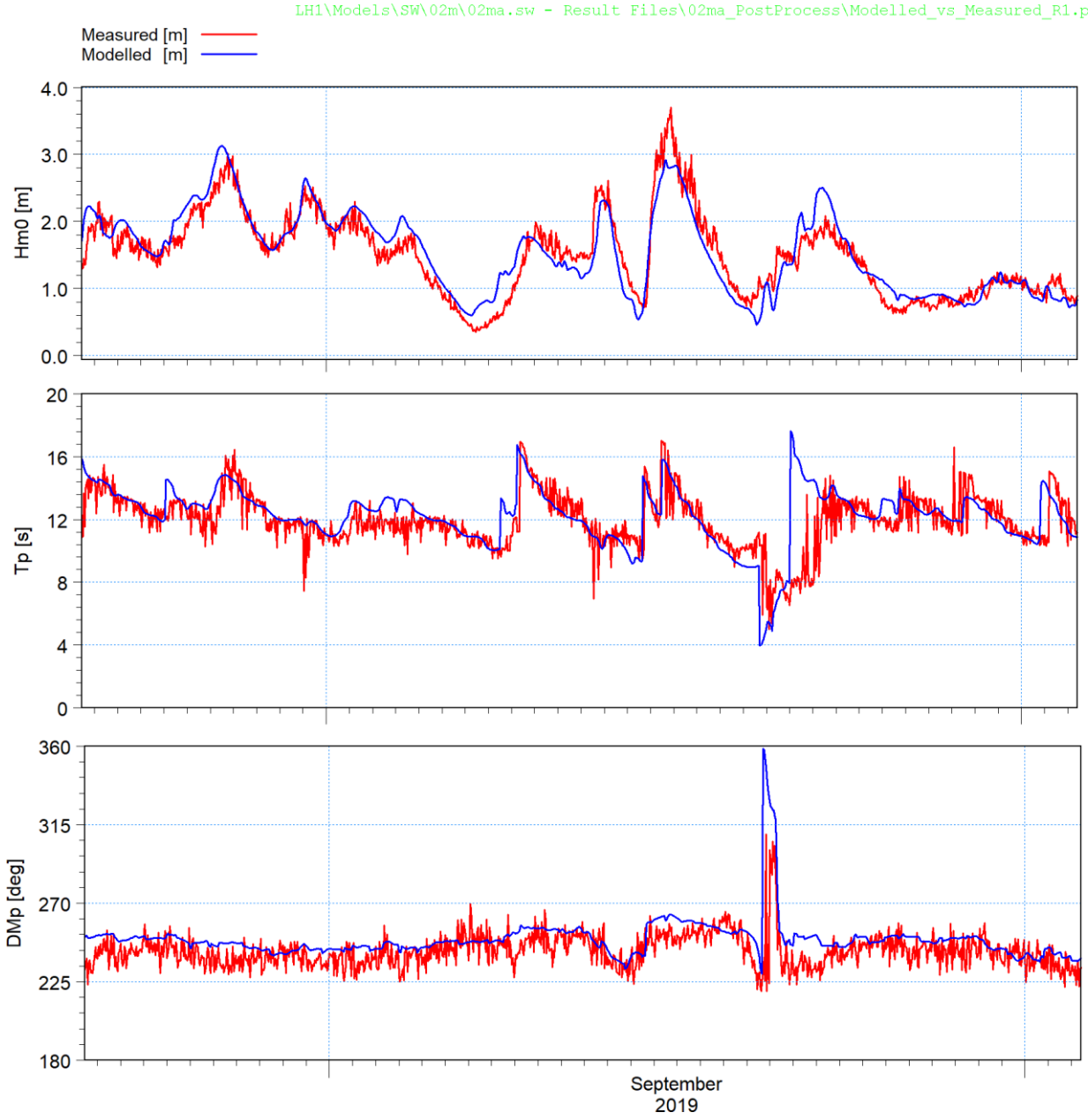

Figure 4-4: Winter/spring: Timeseries of measured and modelled H_{m0}, T_P and D_{MP} at the location of the ADCP.

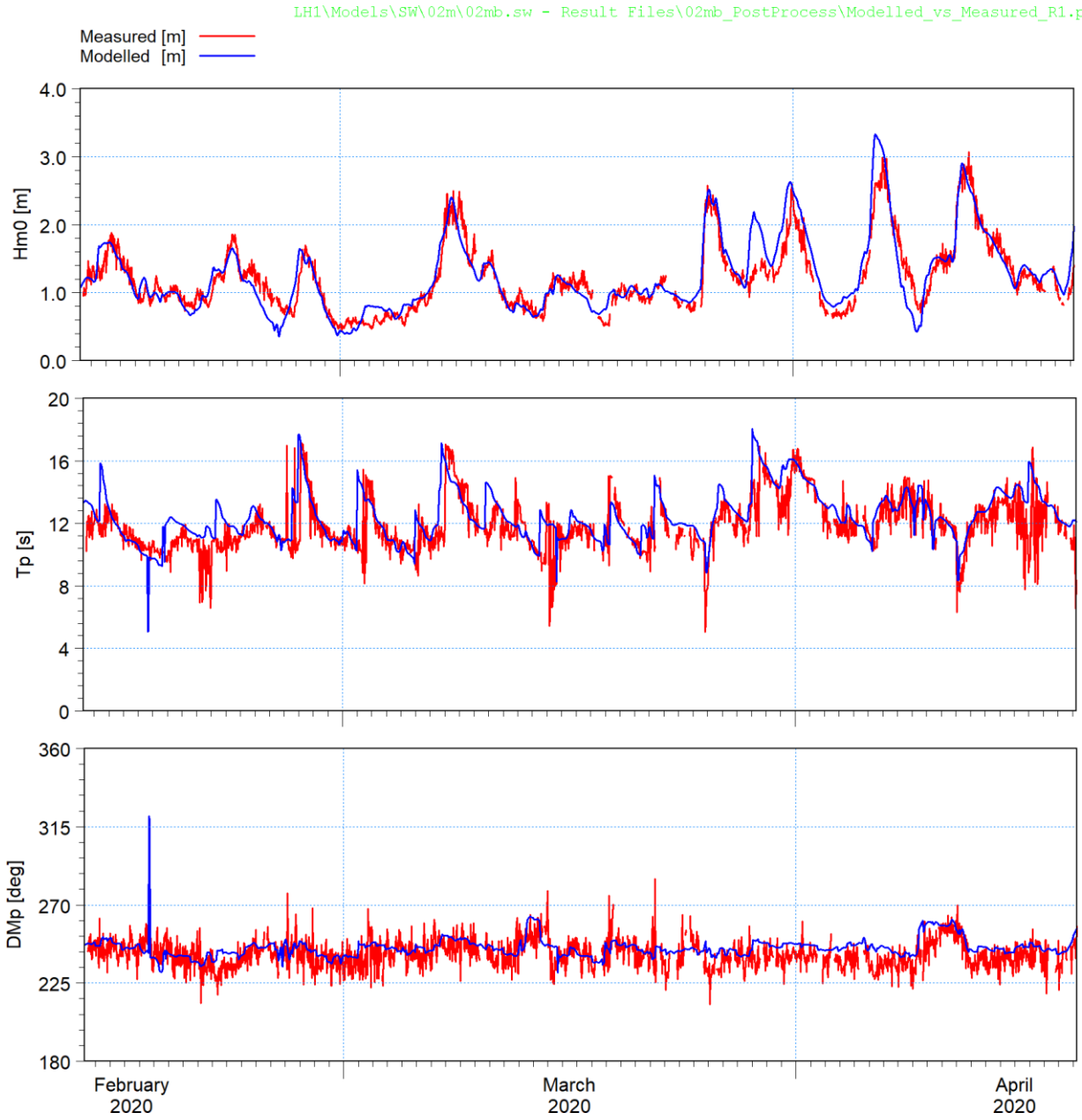

Figure 4-5: Summer/autumn: Timeseries of measured and modelled H_{m0}, T_P and D_{MP} at the location of the ADCP.

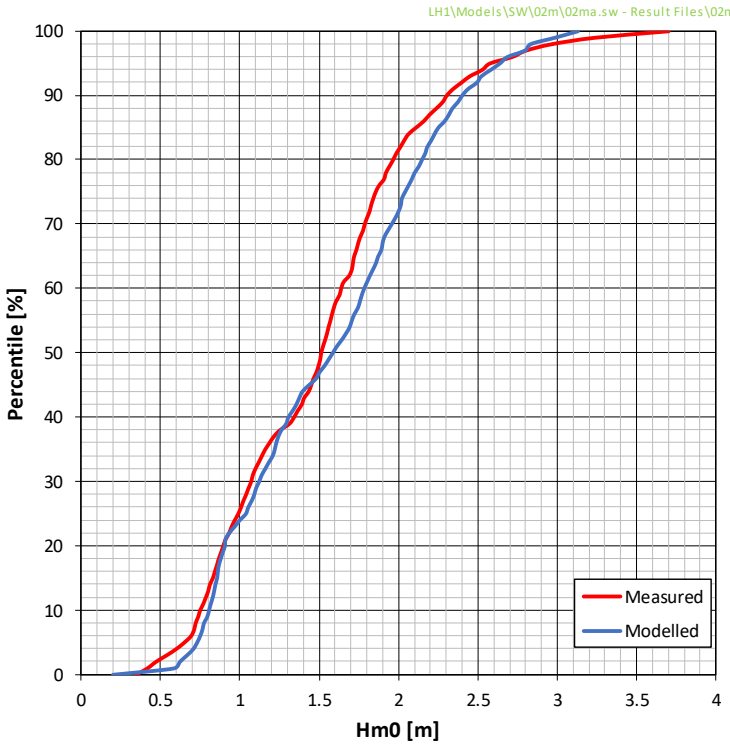

Percentile [%]	Hm0 [m] Measured	Hm0 [m] Modelled
10	0.75	0.81
20	0.90	0.91
30	1.07	1.12
40	1.34	1.31
50	1.51	1.59
60	1.64	1.78
70	1.79	1.96
80	1.97	2.15
90	2.30	2.40
95	2.58	2.64
99	3.24	2.99

Figure 4-6: Winter/spring: Percentile plot for the measured and modelled H_{m0} for the 6-week deployment period at the location of the ADCP.

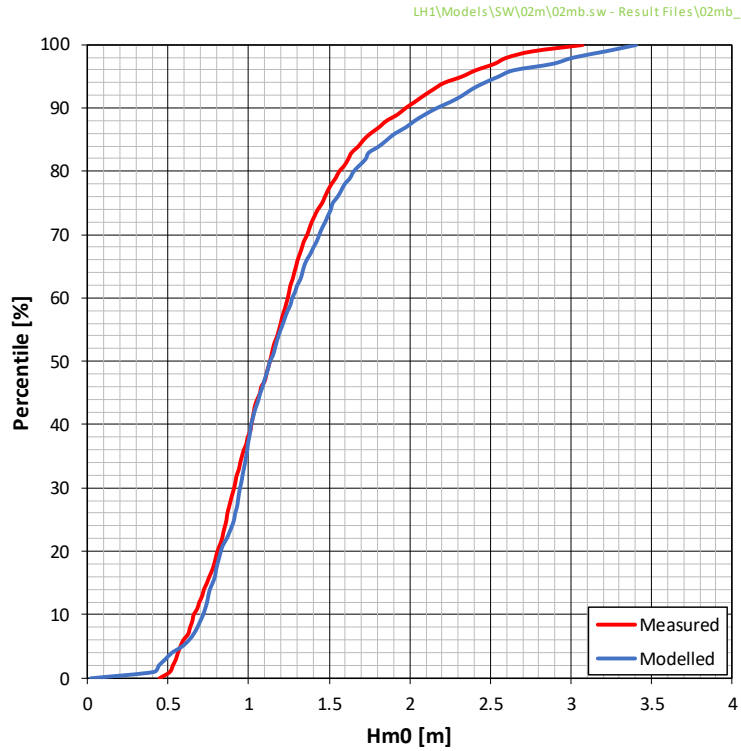

Percentile [%]	Hm0 [m] Measured	Hm0 [m] Modelled
10	0.66	0.71
20	0.80	0.82
30	0.91	0.94
40	1.01	1.01
50	1.13	1.13
60	1.24	1.27
70	1.36	1.44
80	1.56	1.65
90	1.97	2.16
95	2.32	2.55
99	2.76	3.22

Figure 4-7: Summer/autumn: Percentile plot for the measured and Hm0 for the 10-week deployment period at the location of the ADCP.

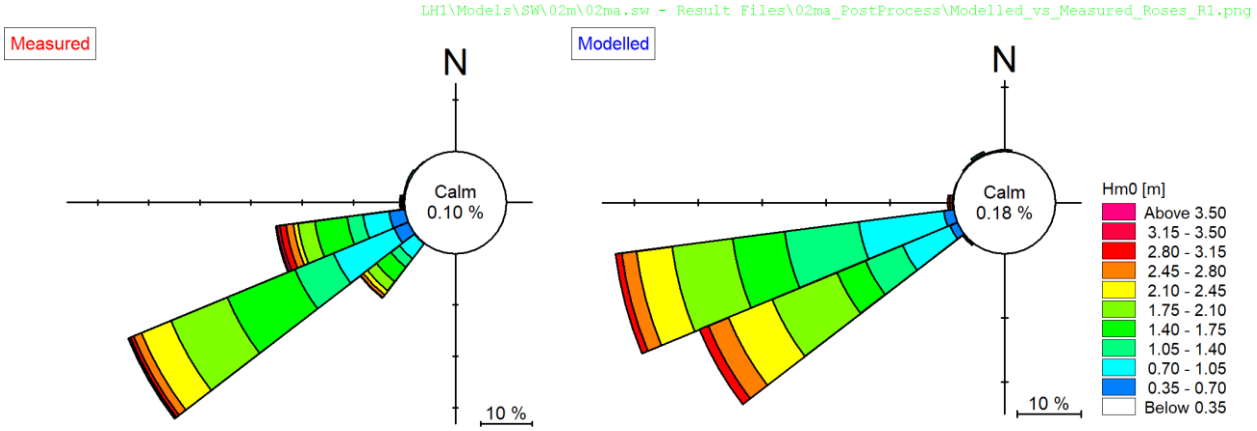

Figure 4-8: Winter/spring: Wave roses of measured and modelled H_{m0} for the 6-week deployment period at the location of the ADCP.

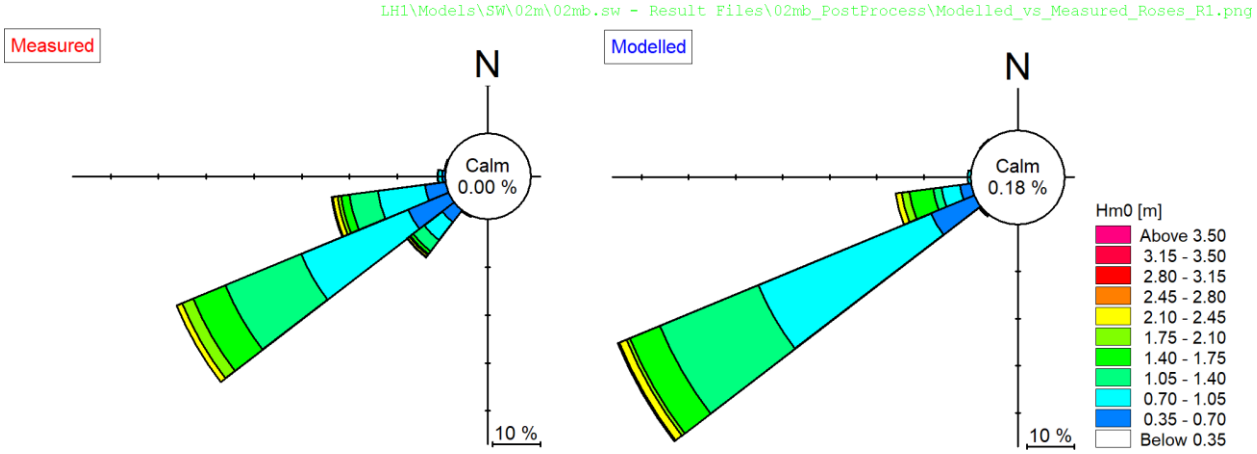

Figure 4-9: Summer/autumn: Wave roses of measured and modelled H_{m0} for the 10-week deployment period at the location of the ADCP.

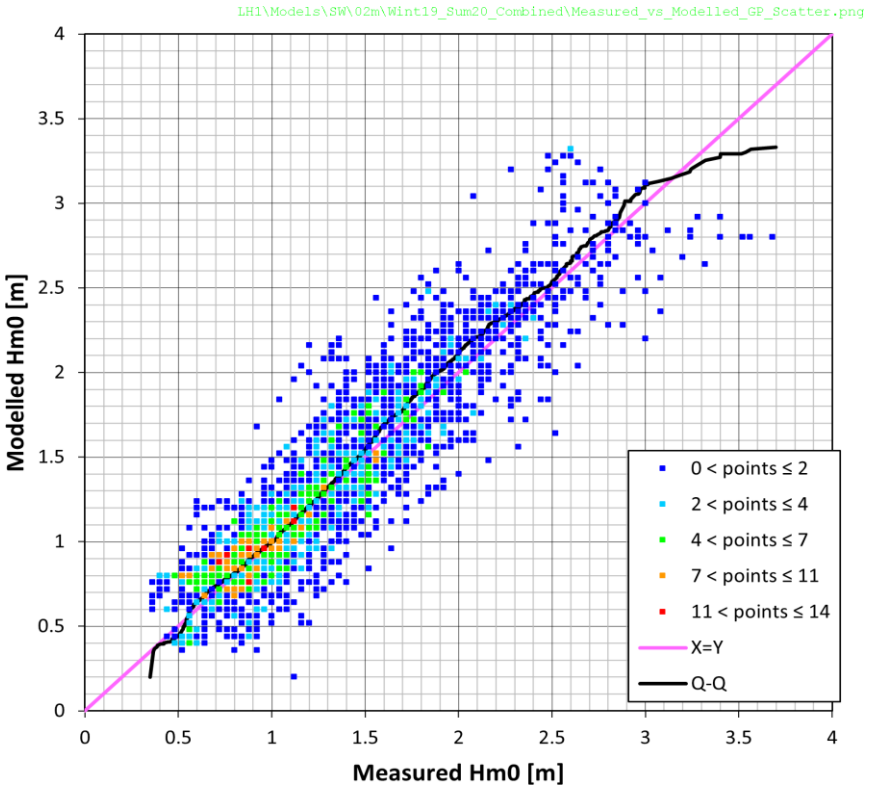

Figure 4-10: Measured versus modelled H_{m0} for Winter/Spring 2019 and Summer/Autumn 2020 combined.

A good overall comparison can be observed from the timeseries, wave rose and percentile plots. Occasional over- or underprediction of wave heights can be observed, but there is no bias. The modelled peak wave period compared well to the measurements. The modelled wave direction showed a small constant offset of about 5˚ compared to the measurements. The agreement between the ADCP measurements and the wave model outputs shows the model to be adequately calibrated for the purpose of this study.

4.5 Storm selection

For the extreme wave climate, modelling the full 42.05 years of available data was not necessary. Rather, a series of storms was selected from a timeseries of hindcast wave data at the offshore node closest to the project site. The storm peaks were identified using the 'partial duration series' method to identify an average of five storms per year. Storms were selected based on total wave height and on wave energy in the north-westerly sector, resulting in a total selection of 361 storm events (after removing overlapping storms from the two sets). To ensure independence, the inter-event time was set to 48 hours. Initial model results from a less refined model were used to select a subset of the 361 storms by identifying the 168 largest storms per year i.e. four per year on average. Each of the 168 storm events was then modelled for a duration of 36 hours before and 24 hours after the offshore storm peak.

4.6 Results

4.6.1 Wave results

Figure 4-11 presents a wave refraction plot for the 13 July 2020 storm event and the location of P1 at position (X = -55 372 m, Y = -3 751 980 m) at the -20 m MSL contour where wave parameters were extracted from each of the storm runs.

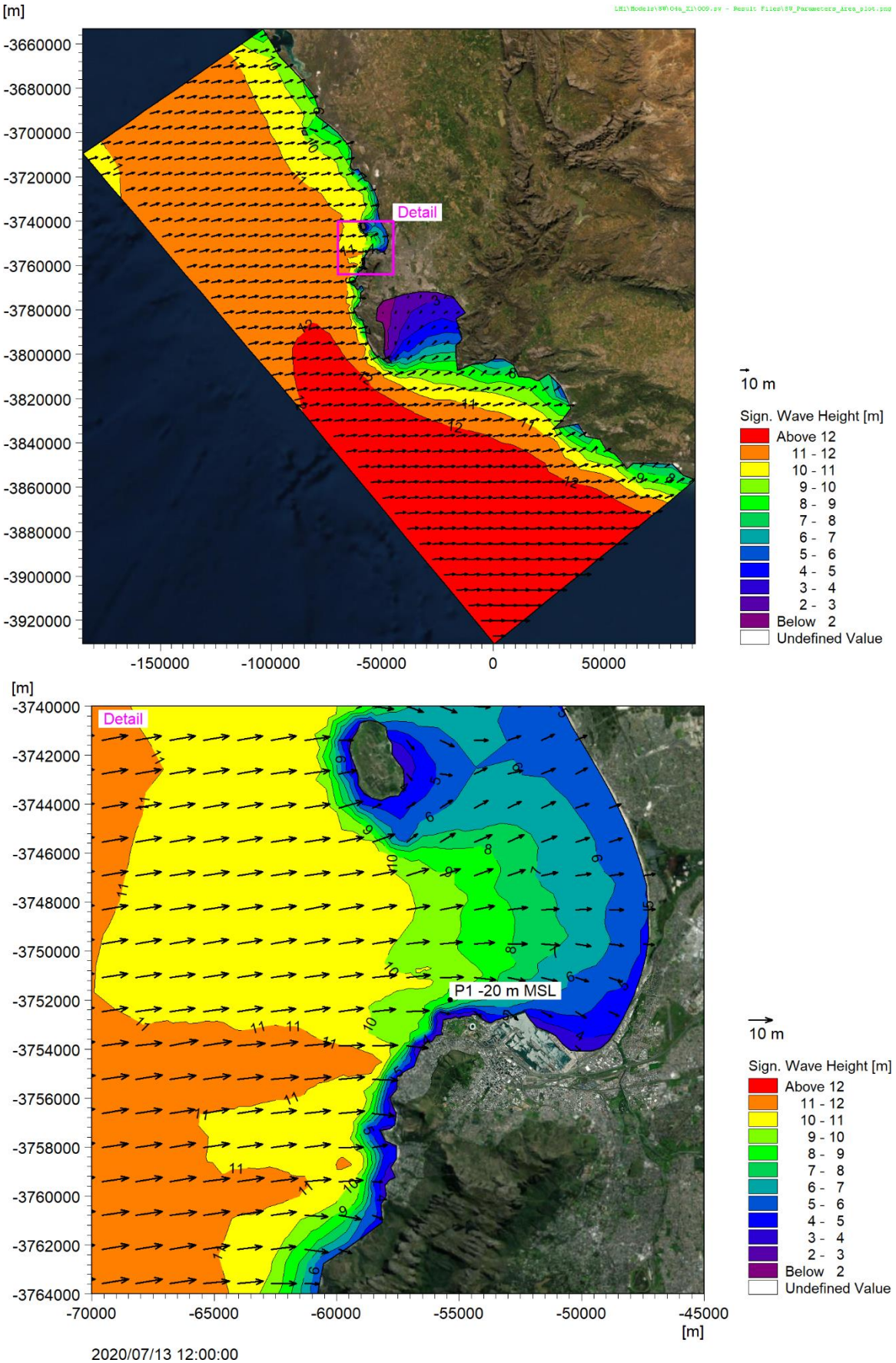

Figure 4-11: Wave refraction plot for the 13 July 2020 storm event.

A directional extreme value analysis (EVA) was performed on the wave heights at P1 using the 'MIKE by DHI' EVA toolbox (DHI, 2024b). The analysis comprises fitting a three parameter Weibull distribution using the Method of Moments to an extreme value series extracted from the input timeseries. The extreme value series was selected using the peaks over threshold method, with the threshold defined as the value that is exceeded once per year on average. To ensure independence, two successive events were extracted only if the time between the events exceeded 48 hours. The uncertainty was calculated using Jack knife resampling to evaluate the mean and standard deviation of the estimate to obtain the 95% confidence (2.5^{th} to 97.5^{th} percentile) estimates.

The results at P1 were separated into six directional bins to test the full range of directional extreme conditions at the site. The directional bins used were: 245 to 285, 285 to 290, 290 to 295, 295 to 300, 300 to 305, and 305 to 310 deg. An EVA plot for the 285 to 290 deg bin is shown Figure 4-12, while Figure 4-13 shows the best estimate curves for all six directional bins.

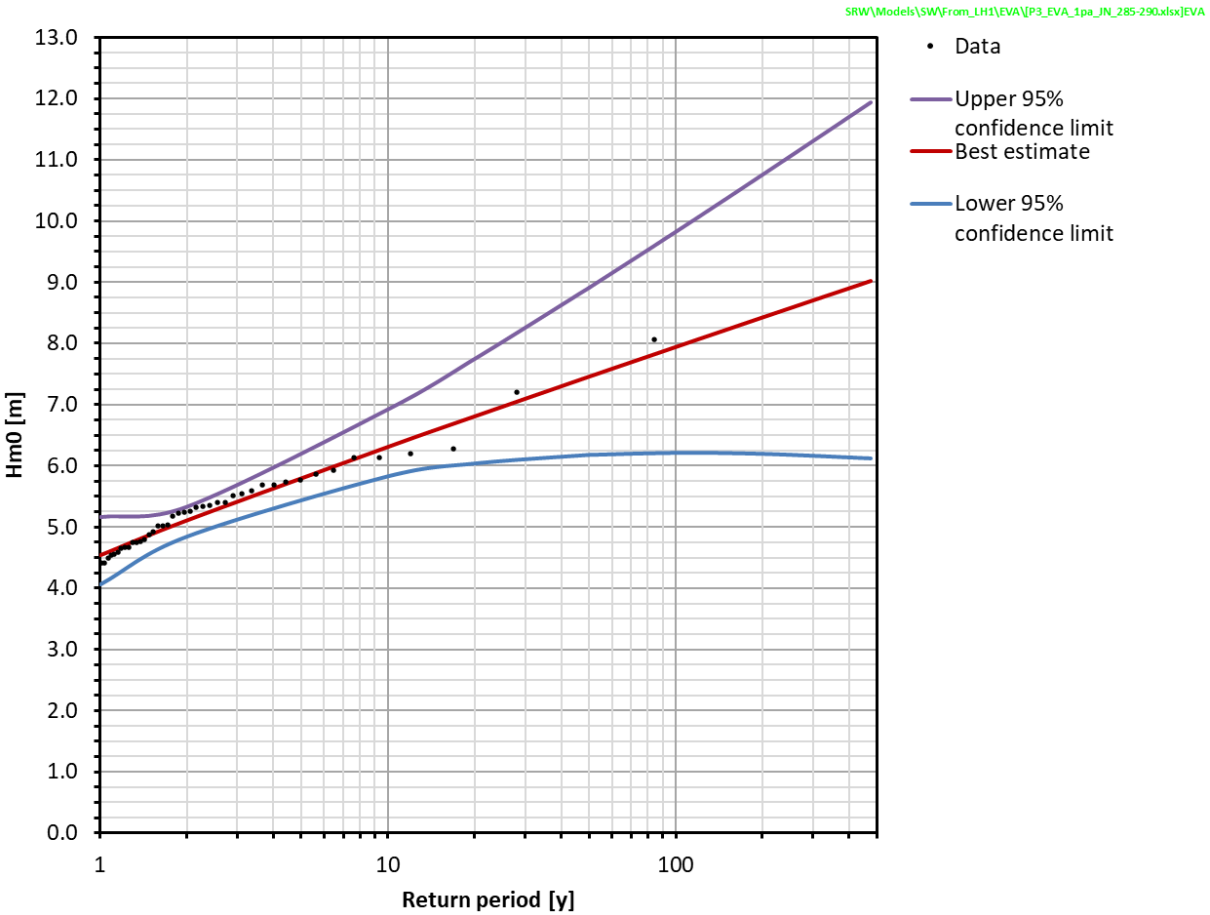

Figure 4-12: H_{m0} EVA plot for the extreme wave climate at P1 for 285 to 290 deg.

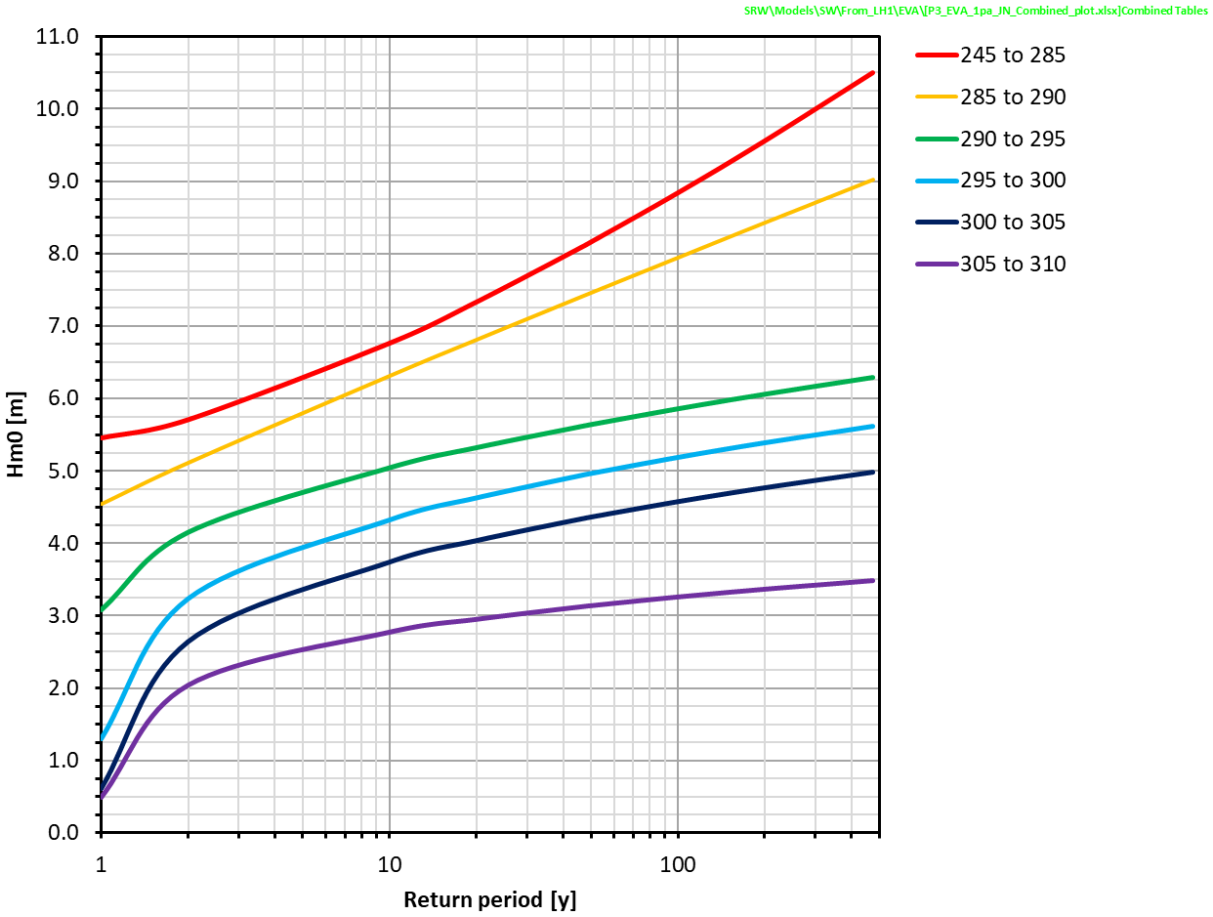

Figure 4-13: Best Estimate H_{m0} EVA plot for the extreme wave climate at P1 for all direction bins.

Figure 4-14 presents a scatter plot of wave parameters (H_{m0}, T_p, D_{MP}, and DSD) constructed from the 168 modelled storms. The D_{MP}-T_p scatter plot shows a clear relationship between wave direction and period, with the longer period swells limited to more westerly directions, while shorter period waves can be more northerly. Granger Bay is sheltered from westerly waves and more exposed to northerly waves.

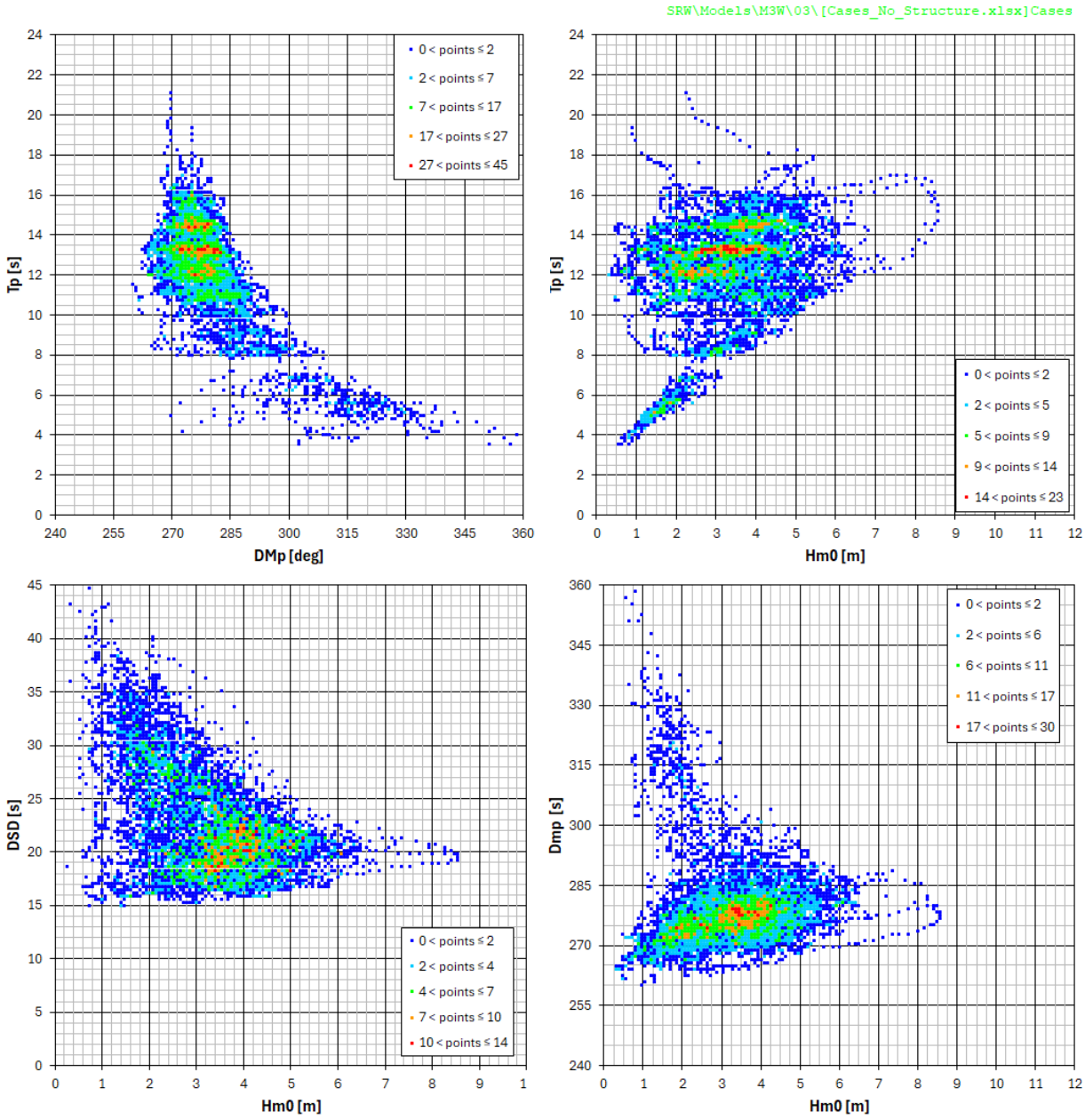

Figure 4-14: H_{m0}, T_p, D_{MP}, and DSD scatter plots at P1.

Table 4-1 presents a summary of the best estimate extreme wave conditions at P1. In addition, a 1-month return period for an omnidirectional case was estimated by selecting the largest independent wave events per year with an average of 12 events per year from a 3-year operational timeseries and selecting the lowest value. A reasonable T_p was selected based on the scatter plot for each case modelled in the wave penetration model. The resulting set of modelled wave cases is shown in Table 5-1.

Table 4-1: Extreme wave conditions at P1 (-20 m MSL).

Return Period[(a)] [y]	H_{m0}[(b)] [m]					
	245-285 deg	285-290 deg	290-295 deg	295-300 deg	300-305 deg	305-310 deg
1	5.5	4.5	3.1	1.3	0.6	0.5
10	6.8	6.3	5.0	4.3	3.7	2.8
50	8.2	7.5	5.6	5.0	4.4	3.1
100	8.8	8.0	5.9	5.2	4.6	3.3
475	10.5	9.0	6.3	5.6	5.0	3.5

(a) Baseline date is 2000. Refer to Table 2-1 for extreme wave height increase due to climate change.
(b) Best estimate.

4.6.2 Joint probability of storm surge and wave height

A methodology for calculating the joint probability and resultant impact on coastal flooding of storm surge vs wave height, storm surge vs river discharge and wave height vs river discharge is described by Petroliagkis, et al. (Joint Probabilities of Storm Surge, Significant Wave Height and River Discharge Components of Coastal Flooding Events. EUR 27824 EN. doi:10.2788/677778, 2016). This methodology has been applied in this section, based on the similarity of the application and the solid theoretical basis presented in Petroliagkis, et al. (Joint Probabilities of Storm Surge, Significant Wave Height and River Discharge Components of Coastal Flooding Events. EUR 27824 EN. doi:10.2788/677778, 2016). The joint (combined) return period of two variables (e.g., storm surge and wave height) is given by:

$$T_{X,Y} = \sqrt{\frac{T_X \cdot T_Y}{\chi^2}} \qquad \textit{Eq 4-1}$$

The dependence parameter χ is calculated from a site-specific dataset containing simultaneous values of the first (X) and second (Y) variables. The methodology requires counting the number of events where both variables simultaneously exceed a common percentile threshold (x^*, y^*), which enables χ to be calculated for each percentile as shown in Eq 4-2:

$$\chi = 2 - \frac{\ln\left[\frac{\text{Number of (X,Y) such that } X \le x^* \text{ and } Y \le y^*}{\text{Total number of (X,Y)}}\right]}{\frac{1}{2}\ln\left[\frac{\text{Number of } X \le x^*}{\text{Total number of X}} \cdot \frac{\text{Number of } Y \le y^*}{\text{Total number of Y}}\right]} \qquad \textit{Eq 4-2}$$

The largest χ is then selected from the range of percentiles representing the more extreme events, e.g., events above the 85th percentile, since only the extreme events are of interest. The applicable formulas and the full details of the methodology are provided in Petroliagkis, et al. (Joint Probabilities of Storm Surge, Significant Wave Height and River Discharge Components of Coastal Flooding Events. EUR 27824 EN. doi:10.2788/677778, 2016). The following categories of dependence are defined:

Table 4-2: Categories of Dependence (Petroliagkis, Voukouvalas, Disperati, & Bildot, 2016).

Dependence Parameter χ	Category
$\chi \le -0.06$	Negative
$-0.05 \le \chi \le 0.05$	Zero
$0.06 \le \chi \le 0.14$	Low
$0.15 \le \chi \le 0.24$	Modest
$0.25 \le \chi \le 0.34$	Well
$0.35 \le \chi \le 0.44$	Strong
$\chi \ge 0.45$	Very Strong

The site-specific dataset used was the hourly measured storm surge at Cape Town (Section 3.1) and hourly offshore wave hindcast data (refer to Section 4.3) at nodes 35.0°S, 18.0°E (1979-2009) and 34.5°S, 18.0°E (2010-2021). Figure 4-15 shows a scatterplot of these data using 230 430 hourly data pairs, equivalent to 26.3 years.

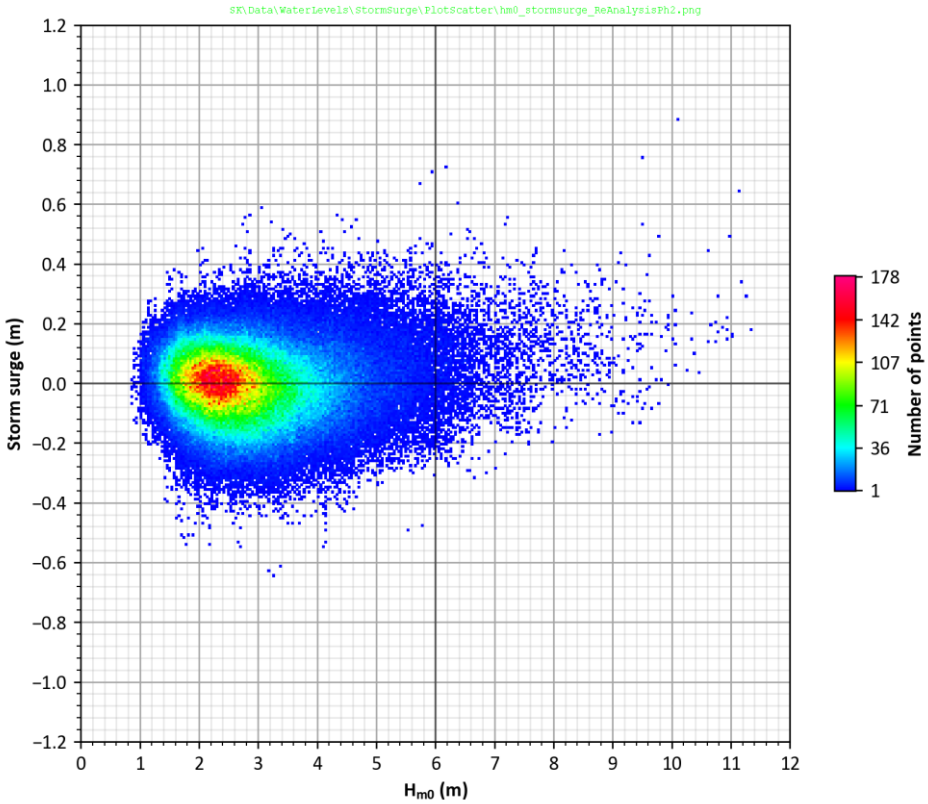

Figure 4-15: Scatterplot of storm surge measured at Cape Town and offshore hindcast wave height.

As shown in Figure 4-15, storm surge and wave height are only moderately correlated at Cape Town, since the frontal weather systems generating the waves hundreds to thousands of kilometres offshore do not arrive at the same time as the waves.

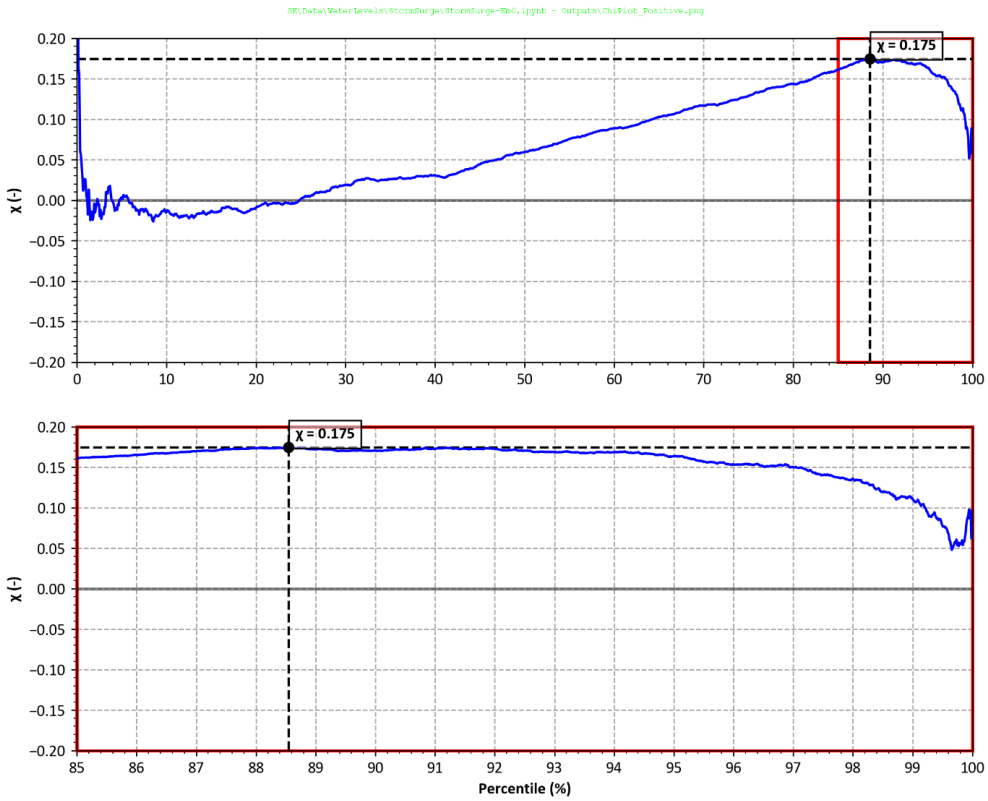

Figure 4-16: Dependence parameter χ of positive storm surge and wave height at Cape Town.

Figure 4-16 shows the calculated dependence parameter χ of positive storm surge and wave height. The results show that χ has a maximum value of 0.175 which is categorised in Table 4-2 as a "modest" dependence. Considering the limited number of extreme storms in the dataset used to calculate χ, the next highest level of dependence has been conservatively applied which is the "well" level of dependence with χ between 0.25 to 0.34 (see Table 4-2).

Selecting $\chi = \frac{1}{\sqrt{10}} = 0.316$ provides a value in the middle the "well" level of dependence, which when applied in Eq 4-1 has the convenient property that the joint return period will have the same return period as variable 1 when combined with a factor 10 lower return period for variable 2, and vice versa. For example, a 475-year joint return period condition can be assessed as a combination of the 475-year return period wave height and 47.5-year return period water level, or vice versa.

5. WAVE PENETRATION AND OVERTOPPING MODELLING

5.1 Model description

The MIKE 3 Wave Model FM (M3WFM) was used to obtain design waves for the new structures, simulate run-up and overtopping of the new structures.

M3WFM is a phase-resolving wave model based on the 3D Navier-Stokes equations and with the free surface described by a height function. The numerical techniques applied are based on an unstructured (flexible) mesh approach. The application of M3WFM is described in the User Manual (DHI, 2024f), while full details of the physical processes being simulated and the numerical solution techniques are described in the Scientific Documentation (DHI, 2024g). The model validation by DHI is described in the Validation Report (DHI, 2024h). PRDW have also validated the model for wave run-up and overtopping using measured data.

The M3WFM model includes the following processes:

- Wave refraction;
- Wave diffraction;
- Bottom friction;
- Non-linear wave transformation;
- Surf and swash zone hydrodynamics;
- Wave breaking and run-up;
- Wave overtopping;
- Coastal flooding; and
- Wave transmission (and reflection) through porous structures.

The model is based on the numerical solution of the three-dimensional incompressible Reynolds-averaged Navier-Stokes equations. Thus, the model consists of continuity and momentum equations, and it is closed by a k-ε turbulence closure scheme in the vertical and horizontal. The free surface is taken into account using a sigma coordinate transformation approach. The spatial discretization of the governing equations in conserved form is performed using a cell-centred finite volume method. The time integration is performed using a semi-implicit scheme. The vertical convective and diffusion terms are discretized using an implicit scheme to remove the stability limitations associated with the vertical resolution. The remaining terms are discretized using a second-order explicit Runge-Kutta scheme. The projection method is employed for the non-hydrostatic pressure. The interface convective fluxes are calculated using a HLLC approximate Riemann solver. This shock-capturing scheme enables robust and stable simulation of flows involving shocks or discontinuities such as bores and hydraulic jumps. This is essential for modelling of waves in the breaking zone or porous structures. The numerical dissipation accounts for the dissipation in the breaking waves.

5.2 Model setup

5.2.1 Bathymetry and mesh

The model bathymetry has been obtained from the following sources:

- CMAP electronic hydrographic charts (DHI, 2024e),
- Available bathymetric surveys in Table Bay,

- Granger Bay hydrographic survey (Underwater Surveys, 2022).

The flexible mesh comprises triangles with a resolution varying between approximately 5 m offshore and approximately 2.5 m around the study area in Granger Bay.

Two layouts were modelled:

- Baseline case: existing layout and structures as in 2024
- Updated development layout for Granger Bay.

A sketch of the new layout is shown in Figure 1-2. Note that only the base structures have been modelled (rock breakwater, rock revetments and slipway without superstructures such as concrete stepped revetments, tidal pools, walkways or piers). The model bathymetry and mesh are presented in Figure 5-1 and Figure 5-2 for the whole domain for the baseline layout. Figure 5-3 to Figure 5-6 present detailed bathymetries and meshes for the study area for the baseline layout and the development layout.

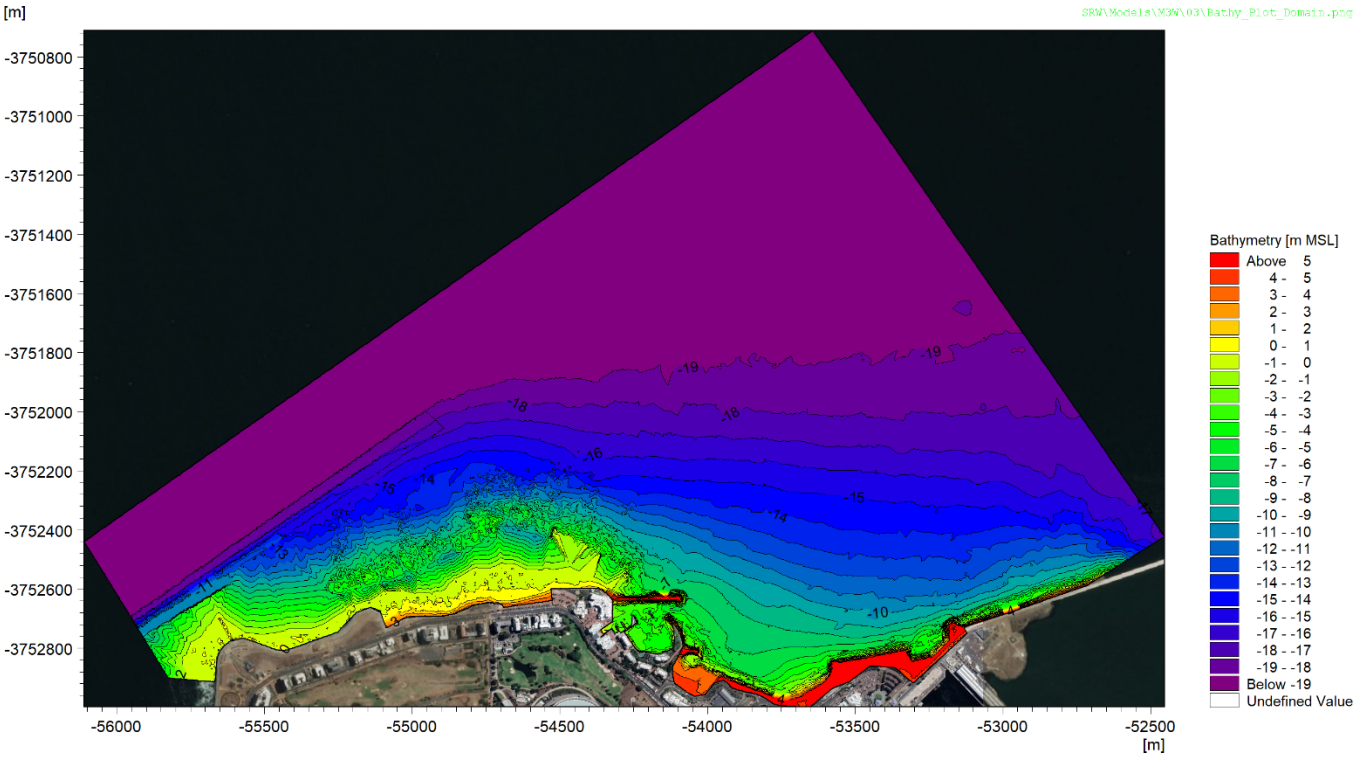

Figure 5-1: Overview of bathymetry for whole domain (baseline layout).

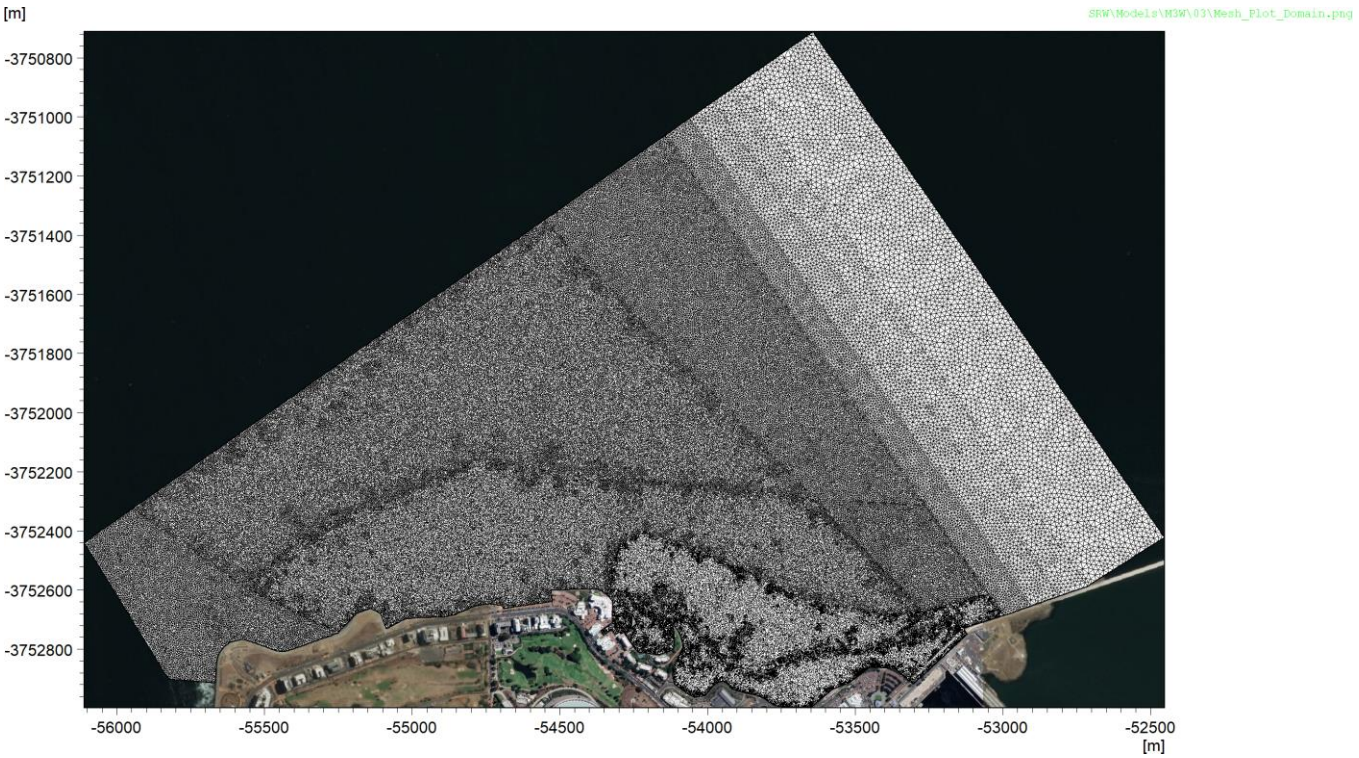

Figure 5-2: Overview of mesh for whole domain (baseline layout).

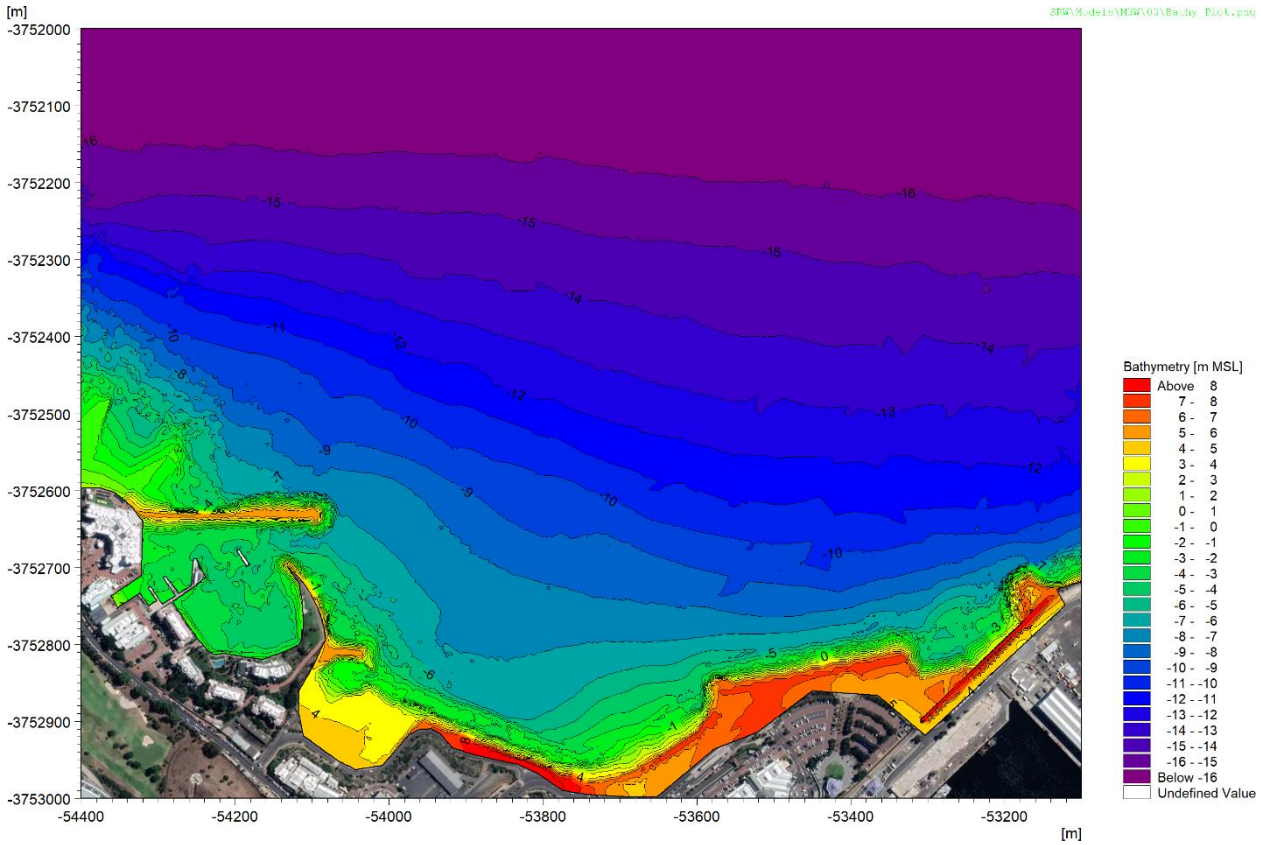

Figure 5-3: Detailed bathymetry for baseline layout.

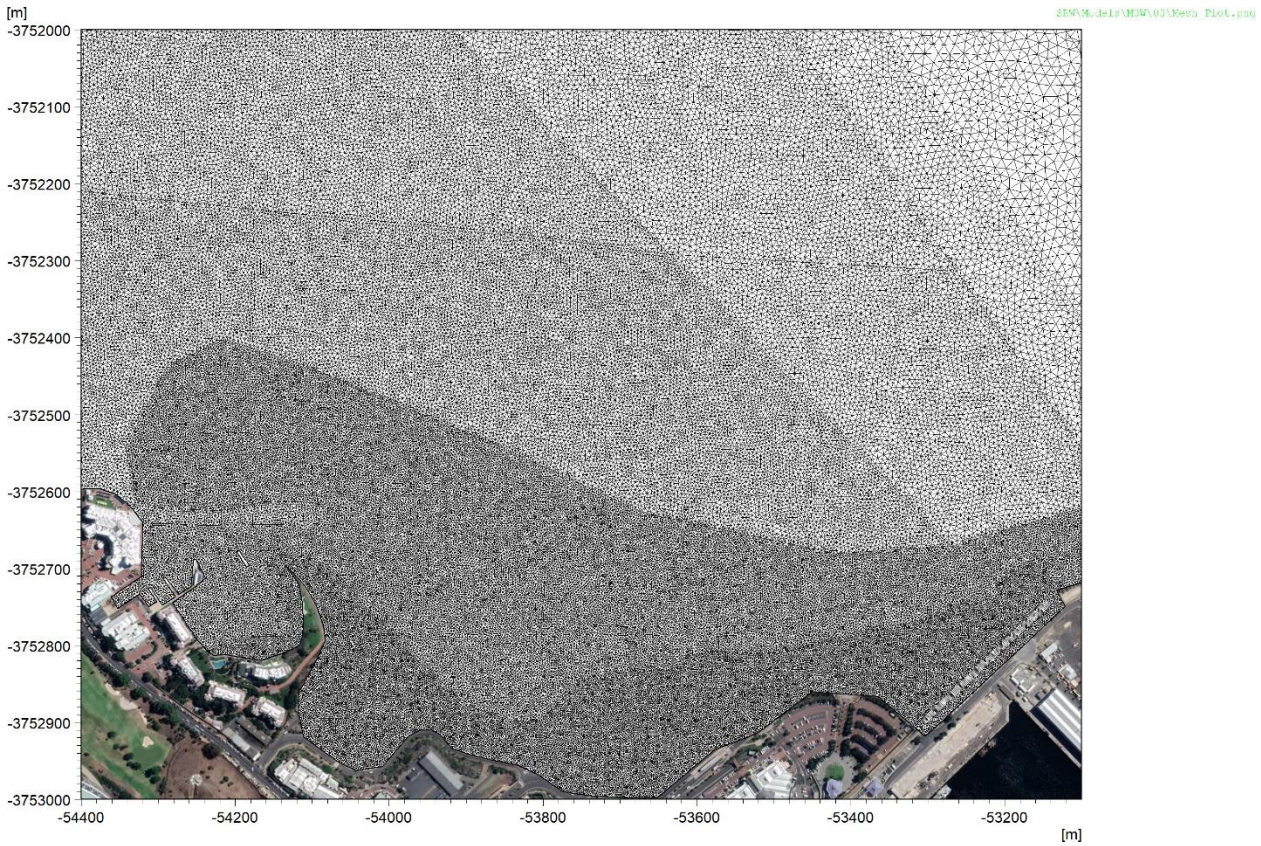

Figure 5-4: Detailed mesh for baseline layout.

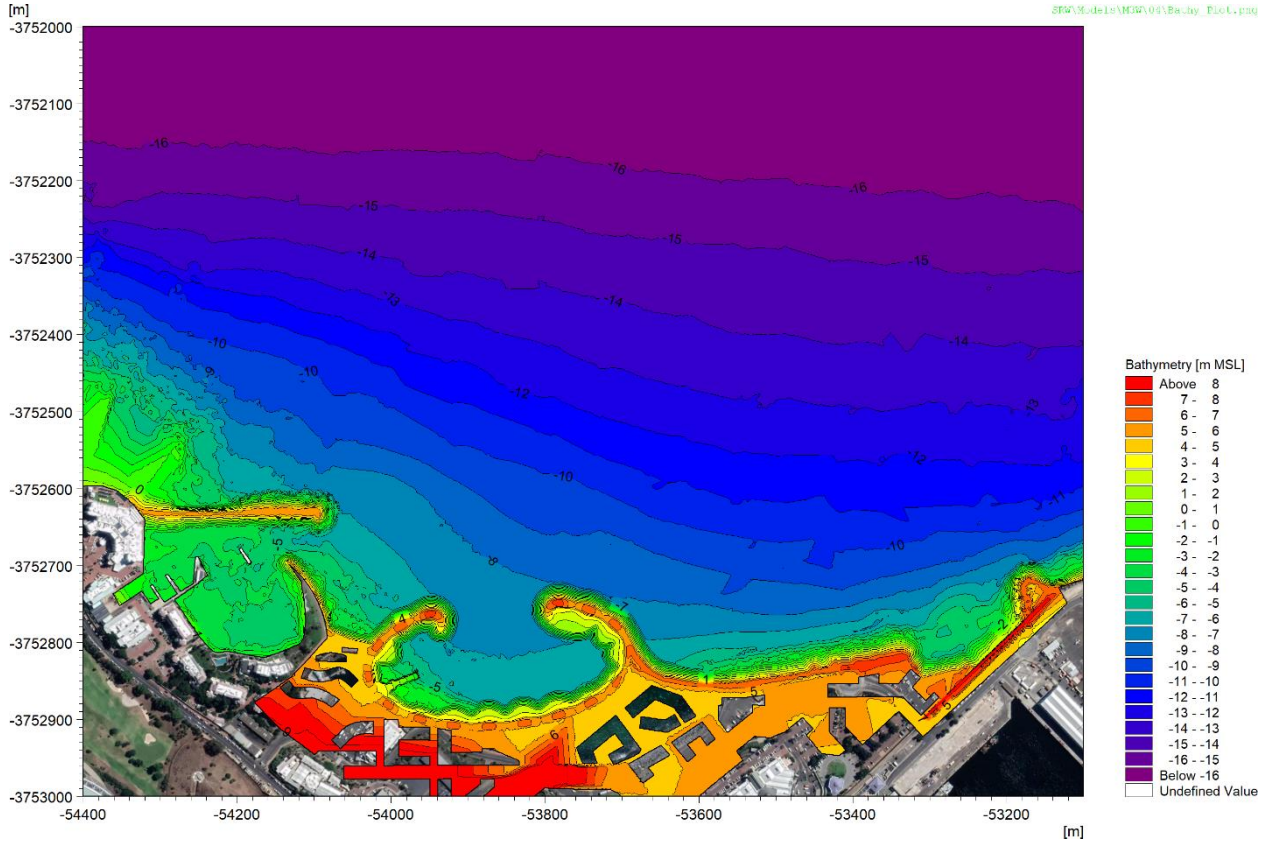

Figure 5-5: Detailed bathymetry for development layout.

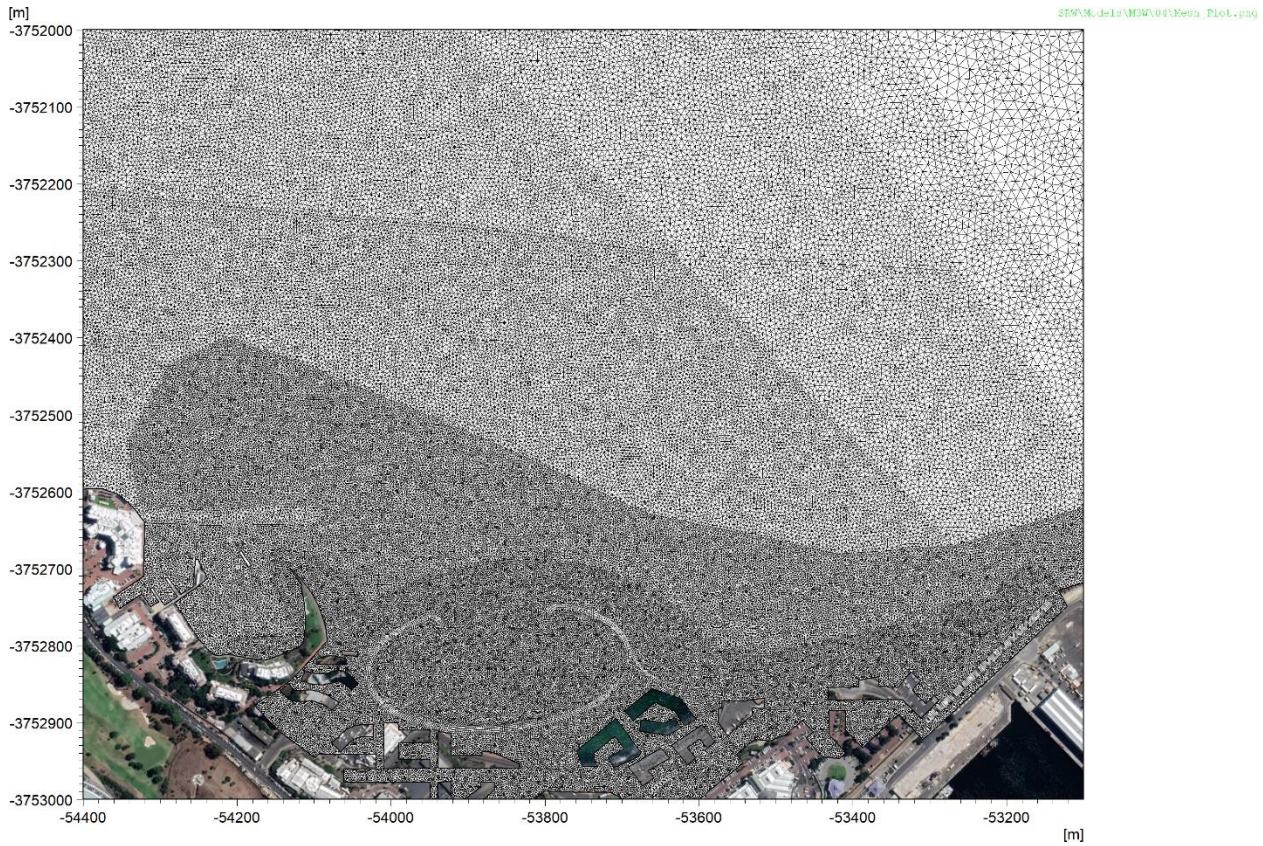

Figure 5-6: Detailed mesh for development layout.

5.2.2 Model inputs

Bottom friction was modelled using the quadratic drag coefficient formulation. The friction coefficient was calibrated to each armouring and structure type in the model (rock slope, dolos slope and rock berm breakwater) by comparing to a detailed, porosity-based M3WFM flume model. The porosity-based model can simulate the resistance of porous structures and more realistically reproduce wave reflection and run-up, however it is computationally intensive to do this at a full 3D scale. Therefore, flume models were used to obtain a calibrated friction value for each type of porous structure.

Each run consisted of 5 minutes of model spin-up and a further 35 minutes of the modelled sea state. The spin-up was ignored in all the results.

Waves in the model were generated at the -20 m MSL contour.

5.2.3 Cases modelled

The cases selected for modelling were chosen to provide inputs for the structural design team and input into the physical modelling.

- 475-year return period conditions to assess overtopping and to provide extreme conditions for design of the coastal structures based on a 10% probability of exceedance over a 50-year design life, as per the design basis for the project (PRDW, 2021).
- 50-year return period conditions to assess how close to the design event a more frequent storm event gets.
- 5-year return period conditions at the beginning of the design life (2024), to assess the stability of coastal structures during construction.
- 1-month return period conditions at the beginning (2024) and end (2074) of the design life to assess the tidal pool and walkway hazards during a typical monthly storm condition.

Based on the nearshore extreme waves and water levels, 14 cases were modelled, including the four return periods described above. Based on the previous modelling and sensitivity tests, only the wave dominated joint probability cases were modelled, with a reasonable T_p assigned based on the H_{m0} vs T_p scatterplots (see Figure 5-7). A constant directional spreading of 20 degrees was applied for all cases. Figure 5-7 presents a 3D scatter plot of modelled nearshore waves with the modelled 475-y return period cases shown.

Table 5-1 presents a summary table of all the cases modelled while Table 5-2 presents the reasoning for each case modelled. Cases 8 to 18 tested the 475-y return period wave conditions for each of the directional bins (refer Section 4.6), with Case 10 being the most critical case for the majority of the development. Subsequent cases were selected based on these results.

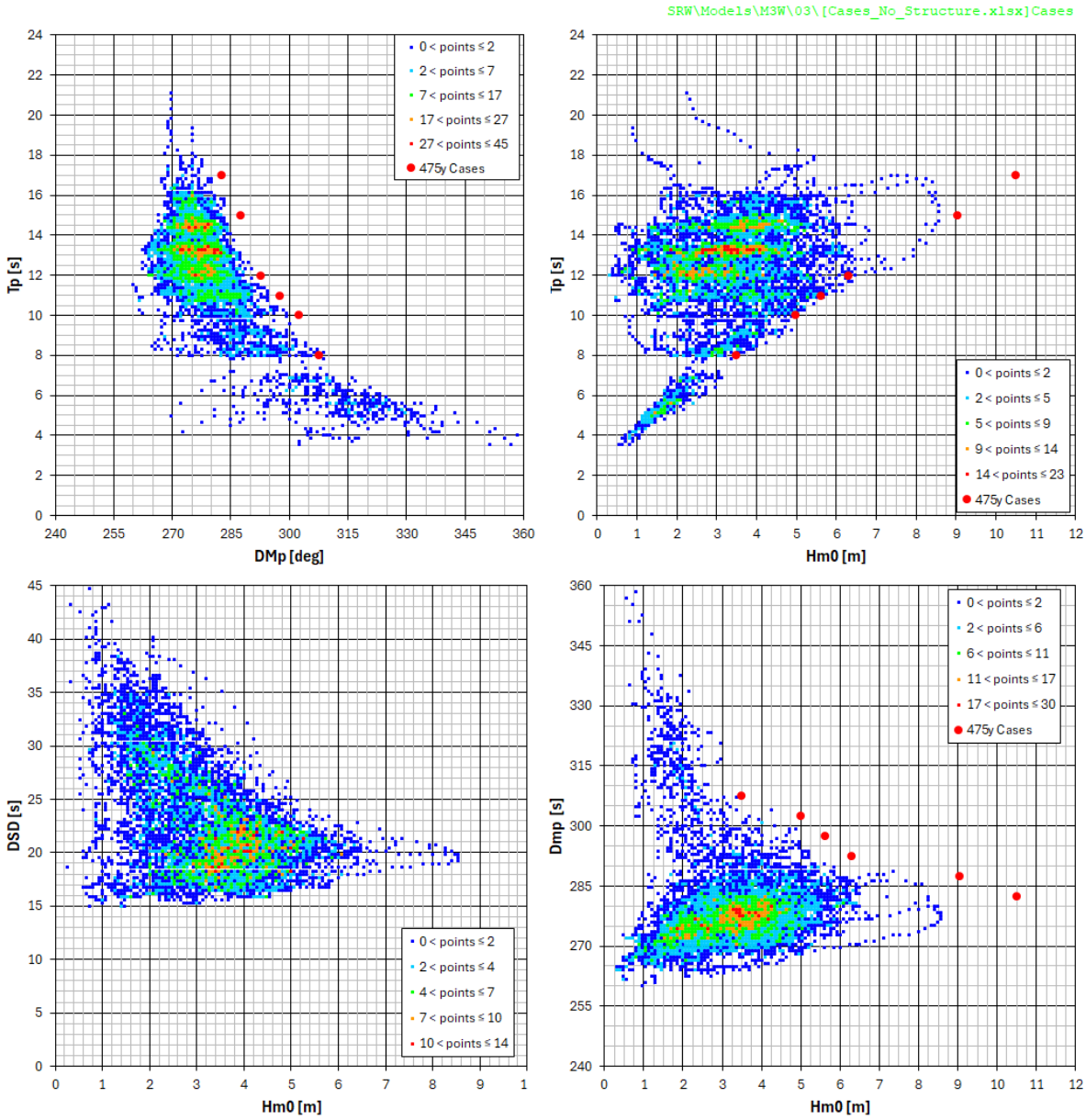

Figure 5-7: Scatter plot of wave parameters at P1 including 475 y cases modelled.

Table 5-1: Modelled cases.

Case	EVA Sector [deg]	Joint Return Period[(a)] [years]	Parameters							Layouts Modelled
			H_{m0} [m]	T_p [s]	D_{mp} [deg]	Tide Level[(b)] [m MSL]	SLR[(c)] [m]	Storm Surge[(d)] [m]	SWL [m MSL]	
8	245 to 285	475	10.49	17	282.5	0.97	0.43	0.75	2.15	Baseline + Structure
10	285 to 290	475	9.03	15	287.5	0.97	0.43	0.75	2.15	Baseline + Structure
12	290 to 295	475	6.29	12	292.5	0.97	0.43	0.75	2.15	Baseline
14	295 to 300	475	5.61	11	297.5	0.97	0.43	0.75	2.15	Baseline
16	300 to 305	475	4.98	10	302.5	0.97	0.43	0.75	2.15	Baseline + Structure
18	305 to 310	475	3.49	8	307.5	0.97	0.43	0.75	2.15	Baseline
10.1[(e)]	285 to 290	475	10.84	15	287.5	0.97	0.43	0.75	2.15	Baseline
10.2[(e)]	285 to 290	475	10.84	15	287.5	-0.53	0.00	0.00	-0.53	Baseline
20	285 to 290	50[(f))]	7.47	15	287.5	0.97	0.43	0.75	2.15	Structure
20.1	285 to 290	50[(f)]	7.47	13	287.5	0.97	0.43	0.75	2.15	Structure
22	285 to 290	5	5.80	15	287.5	0.97	0.02	0.37	1.36	Structure
24	285 to 290	475	9.03	15	287.5	0.20	0.43	0.00	0.63	Structure
26	245 to 285	1 month	3.00	15	282.5	0.95	0.02	0.00	0.97	Structure
27	245 to 285	1 month	3.00	15	282.5	0.95	0.43	0.00	1.38	Structure

Notes:

[(a)] Cases 8 to 18 are wave dominated with the return period of the wave event equal to the joint return period and the storm surge return period a factor 10 lower. Cases 10.1 and 10.2 as well as Cases 20 to 27 were applied with differing water level return periods for various reasons as described in Table 5-2

[(b)] Refer to Table 3-1 for tidal levels

[(c)] Refer to Table 2-1 for SLR values

[(d)] Best Estimate, storm surge. Refer to Table 3-2 for storm surge values

[(e)] Overload Cases where 20% increase in H_{m0} was applied on the boundary

[(f)] Applied with the same extreme water level as for 475 y events to test sensitivity to H_{m0}

Table 5-2: Description of modelled conditions.

Cases	Description
8 to 18	Extreme wave height and water level (including sea level rise). Directions and periods were selected based on measured data. EVAs were conducted on wave heights measured in the directional sector indicated in 4.6.1. Case 8 to Case 18 gradually increases wave direction from 282.5° to 307.5°.
10	This condition resulted in the largest inshore wave heights and is the critical design condition for most of the development.
10.1	This represents a 20% overload of the design condition which is required to check Core-loc stability.
10.2	This represents a 20% overload of the design condition at a low tide which is required to check Core-loc stability toe stability.
20	This represents the same condition as Case 10 with a 50-year return period wave height. This allows an assessment of how much lower inshore wave heights are for such a return period.
20.1	This represents the same condition as case 20 but with a wave period of 13 s, which is more critical for armour rock stability.
22	This represents a condition with the same wave direction and period as Case 10 with a 0.5-year return period surge and 5-year return period wave height. This condition is relevant for the design of lee armour for areas that will remain unprotected until the reclamation has been completed.
24	This represents Case 10 at mean level. It allows an assessment of the significance of water level on storm wave height.
26	An average storm to be expected approximately once per month without sea level rise. This will allow an assessment of overtopping into tidal pools and adjacent amenities for present day conditions.
27	An average storm to be expected approximately once per month with sea level rise. This will allow an assessment of overtopping into tidal pools and adjacent amenities in 50 years' time.

Note that climate change was only applied in the form of SLR and not any increases to waves or storm surge. This was to simplify the comparisons between cases by minimizing the number of variables changing. The SLR was considered to have the greatest effect at the site compared to relatively small increases in storm surge and wave height.

5.3 Model calibration

In the absence of measured water level or wave data in Granger Bay, a qualitative model calibration was undertaken by simulating a specific storm event and comparing the model results to photographs of wave run-up and overtopping taken at the corresponding date and time.

The storm of 13 July 2020 was used for the model calibration. A 1-hour sea state at 15:00 (UTC+2) was modelled using the offshore wave conditions at -20 m MSL obtained from the wave refraction model and measured water levels from Cape Town (described in Section 3.1). The model input conditions are presented in Table 5-3.

Table 5-3: Model inputs at 15:00 for the 13 July 2020 storm.

H_{m0} [m]	T_p [s]	MWD [deg]	DSD [deg]	Water Level [m MSL]
8.0	16.9	276	16	0.1

Figure 5-8 presents a snapshot of the instantaneous surface elevations during the 13 July 2020 storm. This can be compared to Figure 5-9 and Figure 5-10 which show photographs of overtopping along the rock revetment and in front of the Grand Africa Café, respectively.

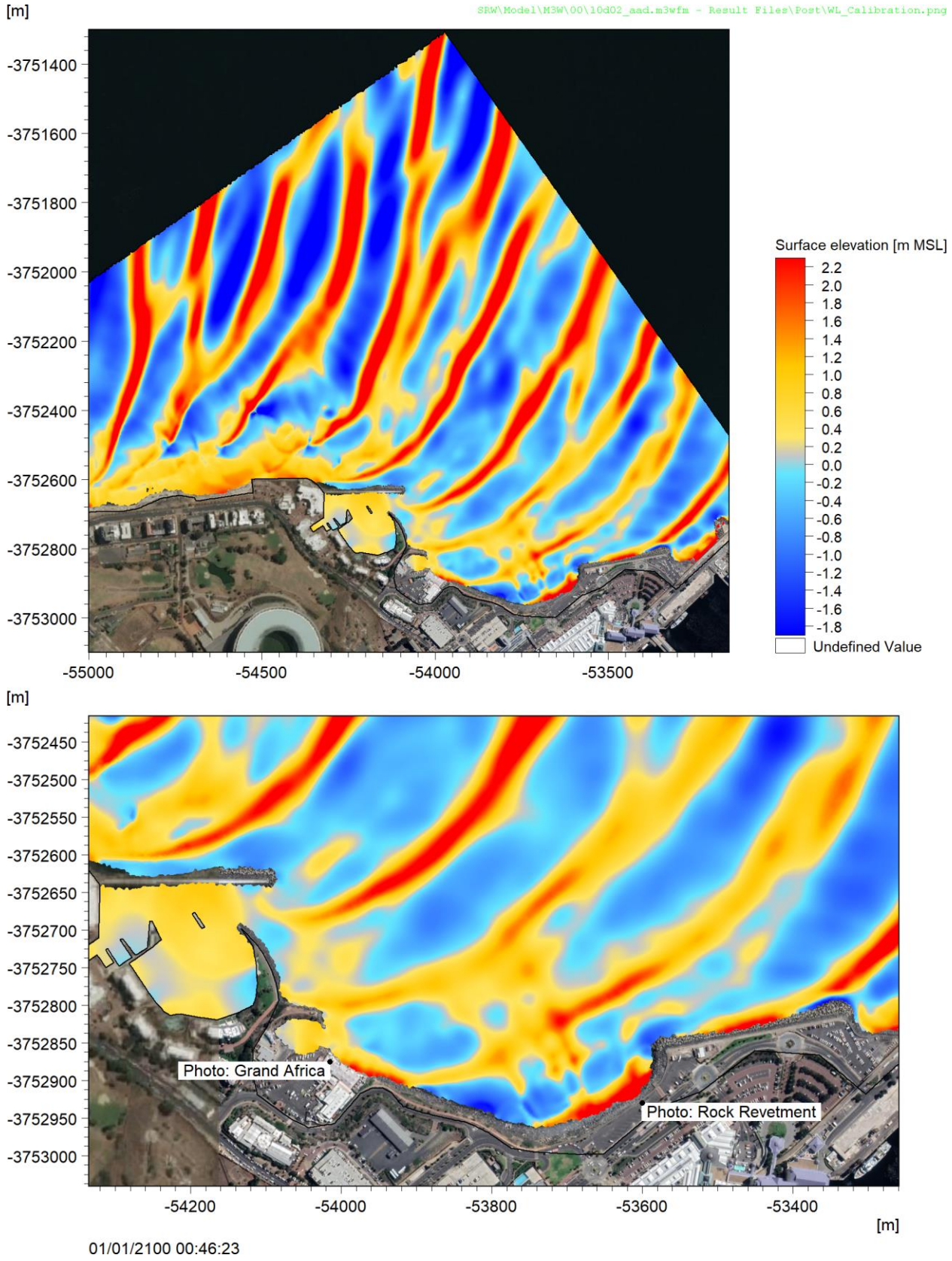

Figure 5-8: Instantaneous modelled surface elevation of an overtopping event during the 13 July 2020 storm.

Figure 5-9: Overtopping of rock revetment at approximately 15:00 on 13 July 2020. Photo credit: Stephen Luger.

Figure 5-10: Overtopping in front of Grand Africa Café on 13 July 2020 (exact time unknown). Photo credit: Anton Holtzhausen.

The snapshot presented in Figure 5-8 shows similar overtopping to the photos taken during the storm at both locations. Although this is not a quantitative comparison, this suggests that the model is accurately reproducing all the processes and as such can be considered to be sufficiently accurate for the purposes of this study.

5.4 Results

5.4.1 Output locations

Figure 5-11 presents the various output locations for the models. The initial runs provided outputs at the original points used in the previous phase of the wave modelling (PRDW, 2022). These are shown as pink squares in Figure 5-11. After the initial runs, two new sets of output points were defined: the outside points, consisting of 24 points outside the development; and the inside points, consisting of 40 points along the inside revetment of the development. The coordinates of each point are provided in Table 5-4.

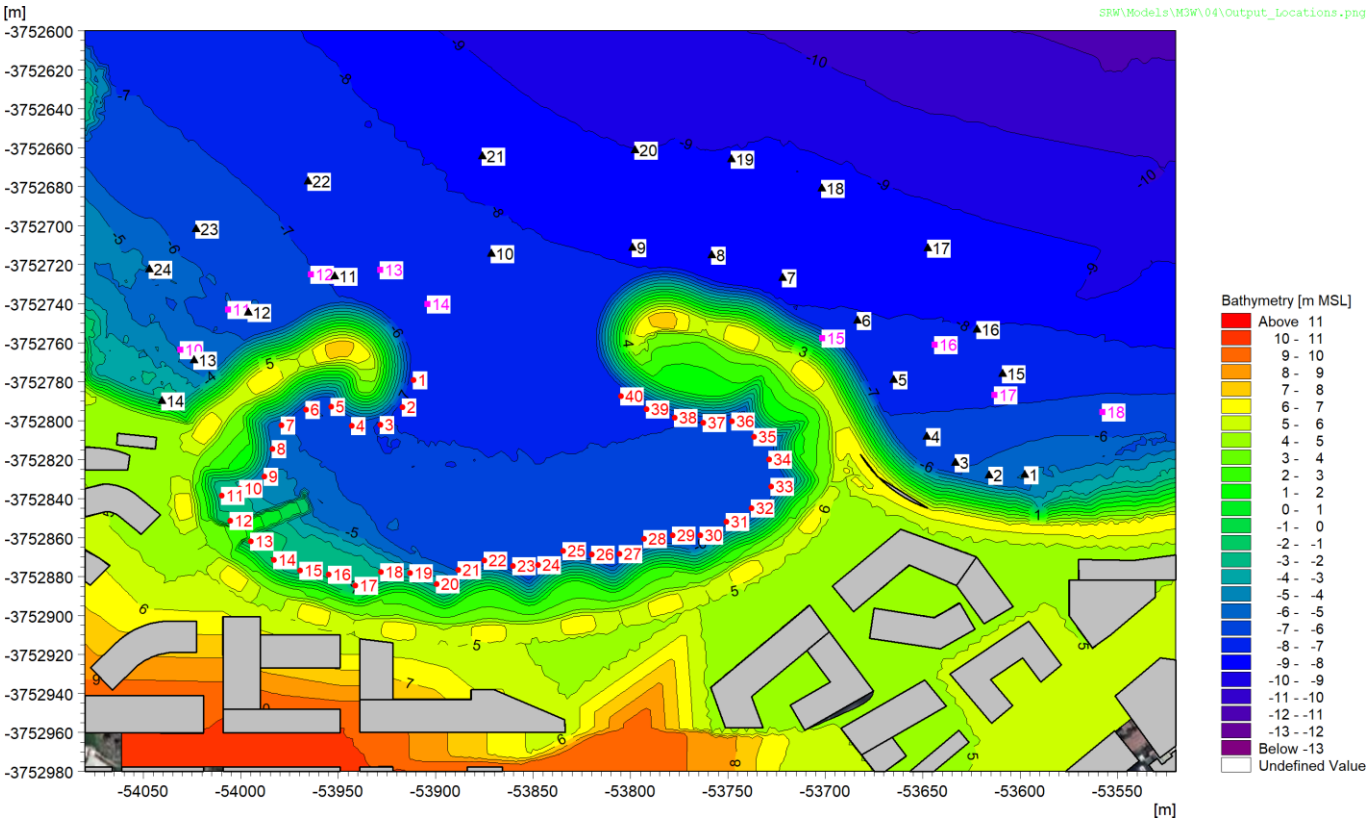

Figure 5-11: Output locations. There are 7 original points (pink squares), 24 outside points (black triangles) and 40 inside points (red circles).

Table 5-4: Coordinates of all output points.

Location	Point	X [m WG19]	Y [m WG19]	Location	Point	X [m WG19]	Y [m WG19]
Inside Points	1	-53911.3	-3752779.2	Outside Points	1	-53597.6	-3752827.9
	2	-53917.0	-3752793.0		2	-53616.1	-3752828.2
	3	-53928.4	-3752802.2		3	-53633.1	-3752821.6
	4	-53943.2	-3752802.6		4	-53647.9	-3752808.4
	5	-53953.8	-3752792.8		5	-53665.0	-3752779.0
	6	-53966.7	-3752794.4		6	-53683.5	-3752748.8
	7	-53979.3	-3752802.4		7	-53721.9	-3752726.9
	8	-53983.8	-3752814.5		8	-53758.3	-3752715.3
	9	-53987.9	-3752828.7		9	-53799.1	-3752711.5
	10	-54000.5	-3752834.9		10	-53871.5	-3752714.4
	11	-54009.8	-3752838.4		11	-53951.9	-3752726.0
	12	-54005.5	-3752851.5		12	-53996.2	-3752744.7
	13	-53994.9	-3752862.0		13	-54024.2	-3752769.1
	14	-53983.2	-3752871.4		14	-54040.5	-3752790.1
	15	-53969.7	-3752877.0		15	-53608.9	-3752776.0
	16	-53955.0	-3752879.0		16	-53622.0	-3752753.5
	17	-53941.2	-3752884.5		17	-53647.5	-3752711.7
	18	-53928.1	-3752877.5		18	-53701.8	-3752680.9
	19	-53913.2	-3752878.1		19	-53748.3	-3752666.1
	20	-53899.6	-3752883.9		20	-53797.7	-3752661.4
	21	-53888.5	-3752876.7		21	-53876.1	-3752664.5
	22	-53875.0	-3752871.8		22	-53965.4	-3752677.4
	23	-53860.3	-3752874.7		23	-54023.1	-3752701.7
	24	-53847.4	-3752874.0		24	-54046.9	-3752722.6
	25	-53834.5	-3752866.9	Original Points	10	-54030.9	-3752763.8
	26	-53819.8	-3752868.6		11	-54006.6	-3752743.1
	27	-53805.8	-3752868.3		12	-53963.9	-3752725.1
	28	-53793.2	-3752860.6		13	-53928.5	-3752722.8
	29	-53778.5	-3752858.8		14	-53904.1	-3752740.3
	30	-53764.1	-3752858.9		15	-53701.6	-3752757.8
	31	-53750.8	-3752852.0		16	-53643.8	-3752761.0
	32	-53737.8	-3752844.9				
	33	-53727.7	-3752833.8				
	34	-53728.8	-3752819.9				
	35	-53736.6	-3752808.3				
	36	-53747.9	-3752800.3				
	37	-53762.6	-3752801.1				
	38	-53777.3	-3752798.4				
	39	-53791.7	-3752794.0				
	40	-53804.9	-3752787.4				

Overtopping in the MIKE3 Wave model is measured by water flowing through a defined line section. The edge of the new development was divided into 15 sections where the average overtopping for each section was

calculated for the duration of the run. These sections are shown in Figure 5-12 below. For each section, only the overtopping from the sea to the land was considered, i.e. the down-rush of water after a flooding wave was not counted.

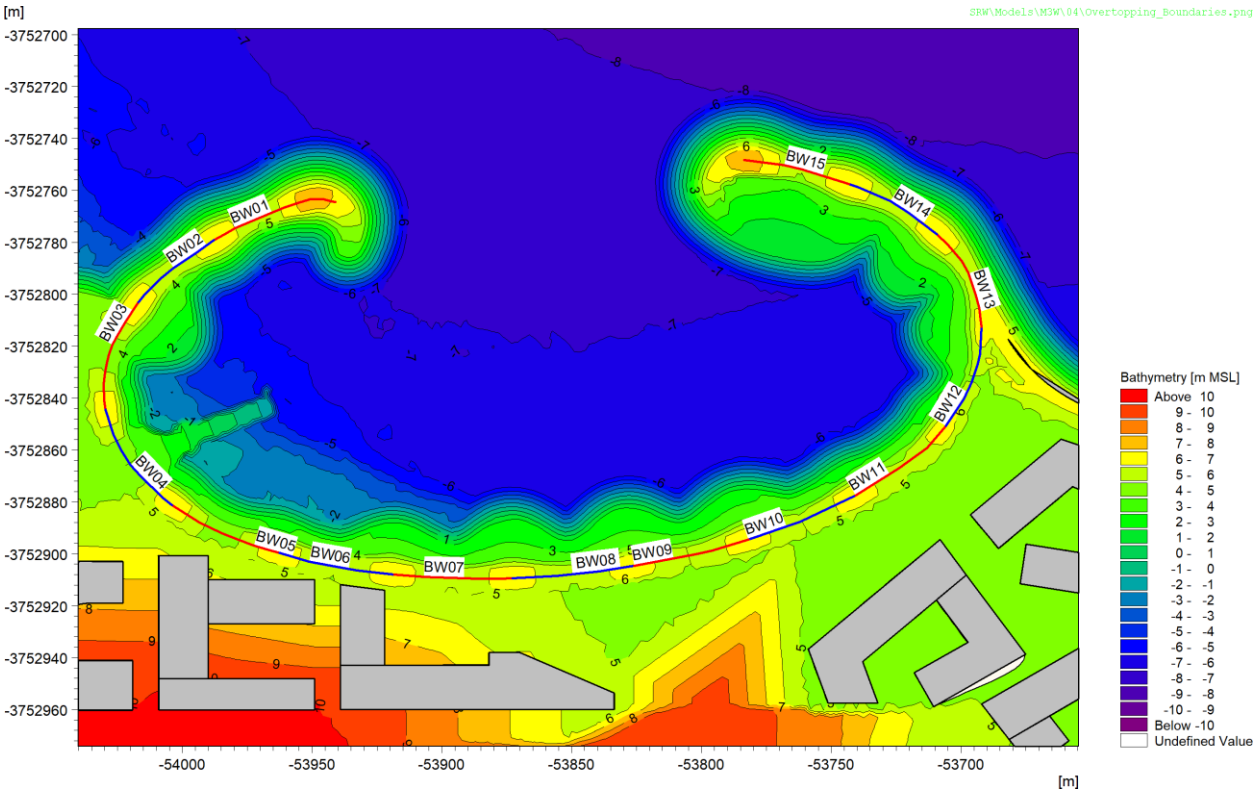

Figure 5-12: Definition of overtopping sections along the proposed new development.

5.4.2 Example wave results

Figure 5-13 and Figure 5-14 present example plots of the significant wave height and an instantaneous snapshot of the waves for the baseline and development layouts, respectively.

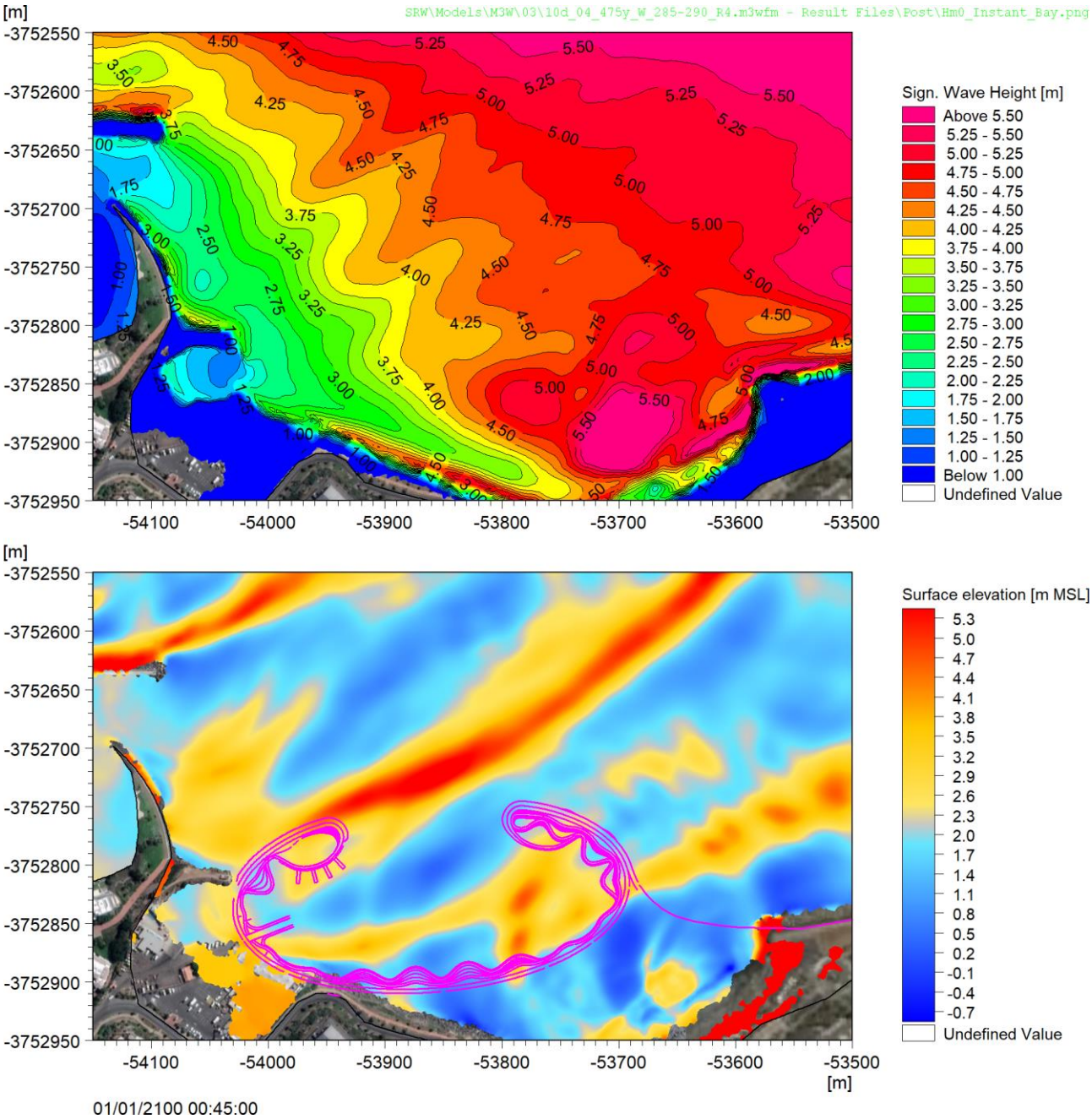

Figure 5-13: H_{m0} and instantaneous surface elevation for the baseline layout, 475-year candidate (Case 10). Boundary conditions: H_{m0} = 9.03 m, T_p = 15 s, Dir = 287.5°, SWL = 2.15 m MSL, SLR for 2074. The development layout is shown in magenta for reference.

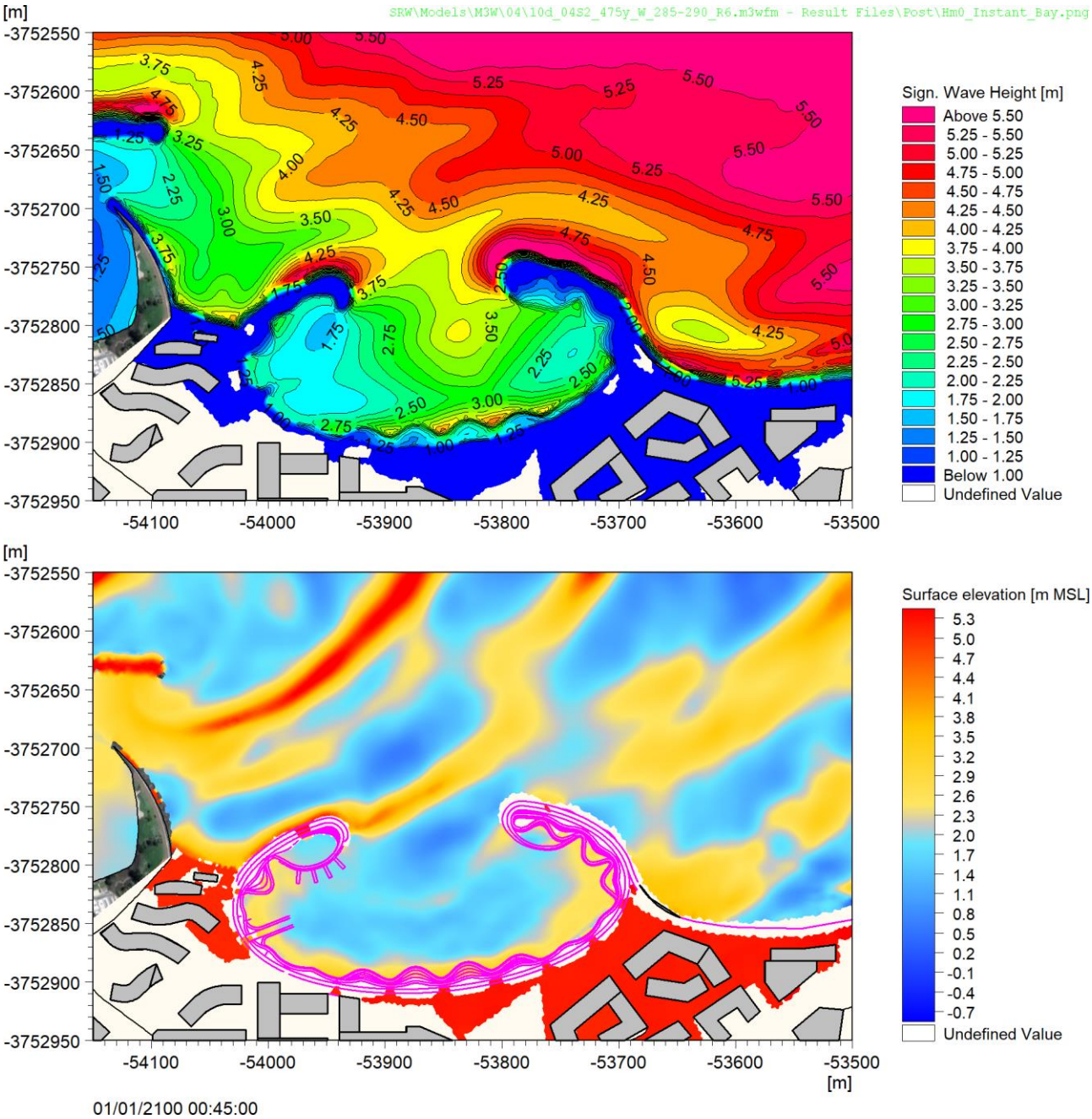

Figure 5-14: H_{m0} and instantaneous surface elevation for the development layout, 475-year candidate (Case 10). Boundary conditions: H_{m0} = 9.03 m, T_p = 15 s, Dir = 287.5°, SWL = 2.15 m MSL, SLR for 2074.

The instantaneous surface elevations and spatial H_{m0} plots for the baseline show reflections off the existing rock revetment at Granger Bay, including the oblique portion adjoining the dolos revetment to the east and the oblique section toward the Oceana. These reflections result in a focusing of wave heights and a local hotspot in the centre of the bay.

The instantaneous surface elevations and spatial H_{m0} plots for the development layout show nodes occurring behind the breakwater heads at the east and west edges of the bay while there is an anti-node in the centre of the bay opposite the entrance. This indicates the presence of long waves inside the basin. These long waves however are not interesting to the structural design of the revetments, nor for input into the physical model. The long waves will have the biggest influence on vessels inside the basin which are not included in the scope

of this study. Long waves will also influence the run-up and overtopping which is included in the overtopping results presented in Section 5.4.4.

Figure 5-15 presents two snapshots of the 3D animation of the wave conditions along the new development Case 10.

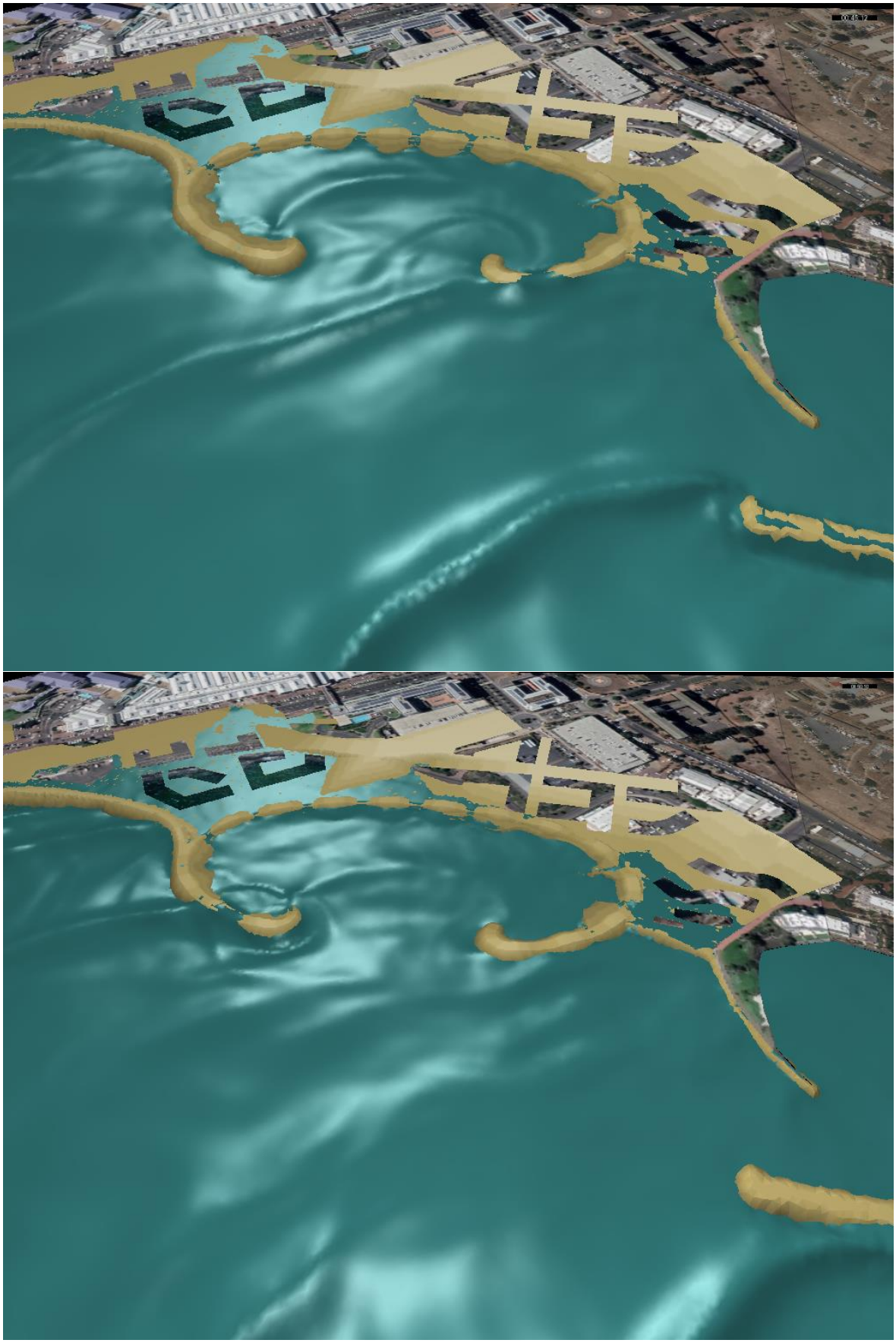

Figure 5-15: 3D snapshots of waves for Case 10 at two different timesteps.

In general, the nearshore wave heights are lower than without the development, due to the additional protection from the breakwaters. The figures above show that the breakwaters provide reasonable shelter in the basin, though significant overtopping occurs during a 475 y storm.

5.4.3 Design waves

Extreme wave heights for design were determined from the model results at the locations shown in Figure 5-11. The waves were calculated by analysing timeseries of the water levels and fluxes to determine the 2D wave spectrum and then separating the incident short and long waves using a 28.5 s cut-off period and appropriate directional cut-offs.

Table 5-5 presents tabulated short wave results for the initial cases at the original points, while Table 5-6 presents the tabulated short wave results for the overload cases at the outside points.

Table 5-5: Short waves (<28.5 s) results for the baseline layout at the original points (see Figure 5-11 for locations of the points and Table 5-1 for the cases).

Point (Original Points)	Incident Short Wave H_{m0} (<28.5 s) [m]					
	Case 8	Case 10	Case 12	Case 14	Case 16	Case 18
10	1.95	2.04	1.61	2.07	2.40	1.80
11	2.36	2.46	1.93	2.32	2.52	1.74
12	3.13	3.12	2.72	3.02	3.19	2.46
13	3.42	3.57	3.06	3.28	3.47	2.50
14	3.52	3.89	3.10	3.33	3.45	2.29
15	3.98	4.32	3.96	4.03	3.28	2.39
16	4.35	4.48	4.11	3.90	3.55	2.35
17	4.29	4.38	4.23	4.08	3.68	2.54

Table 5-6: Overload cases short waves (<28.5 s) results for the baseline layout at the outside points (see Figure 5-11 for locations of the points and Table 5-1 for the cases).

Outside Point	Incident Short Wave H_{m0} (<28.5 s) [m]	
	Case 10.1	Case 10.2
1	5.36	3.74
2	4.84	3.33
3	4.82	3.38
4	4.87	3.45
5	4.58	3.55
6	4.61	3.54
7	4.55	3.60
8	4.52	3.46
9	4.33	3.33
10	4.25	2.90
11	3.59	2.81
12	2.73	2.21
13	2.23	1.80
14	1.98	1.73
15	4.72	3.56
16	4.78	3.56
17	4.97	3.74
18	4.89	3.80
19	4.91	3.76
20	4.76	3.51
21	4.23	3.37
22	4.10	2.82
23	2.80	2.22
24	2.27	1.67

Table 5-7 and Table 5-8 present the short wave results for the cases with the development included at the outside and inside points, respectively.

Table 5-7: Incident short wave (<28.5 s) results for the development layout at the outside points (see Figure 5-11 for locations of the points and Table 5-1 for the cases).

Inside Point	Incident Short Wave H_{m0} (<28.5 s) [m]								
	Case 8	Case 10	Case 16	Case 24	Case 20	Case 20.1	Case 22	Case 26	Case 27
1	3.69	3.42	2.45	3.15	3.27	2.82	2.91	0.89	0.89
2	3.83	3.55	1.96	3.32	3.31	2.83	2.95	1.02	1.03
3	3.63	3.47	1.55	3.33	3.22	2.80	2.99	1.16	1.16
4	3.28	3.19	1.59	2.99	2.90	2.52	2.65	0.94	0.95
5	3.73	3.78	2.07	3.48	3.48	3.09	3.08	1.23	1.23
6	4.28	4.25	2.61	3.78	3.95	3.48	3.38	1.15	1.16
7	4.20	4.20	2.84	3.77	3.90	3.48	3.44	1.27	1.23
8	3.93	4.09	2.94	3.69	3.83	3.49	3.38	1.37	1.28
9	3.61	3.81	3.14	3.43	3.50	3.35	3.14	1.47	1.38
10	3.53	3.81	3.45	3.43	3.68	3.67	3.04	2.00	1.88
11	2.95	2.91	2.91	2.62	2.76	2.53	2.53	1.11	1.12
12	2.04	2.26	1.98	2.07	2.14	1.83	1.82	0.89	0.85
13	1.61	1.68	1.96	1.18	1.62	1.40	1.14	0.58	0.59
14	1.90	2.03	1.08	1.87	2.11	1.59	1.86	0.84	0.86
15	3.92	4.04	3.52	3.66	3.84	3.88	3.34	1.41	1.43
16	4.15	4.10	3.75	3.62	3.82	3.82	3.35	1.38	1.36
17	4.00	4.20	3.78	3.75	3.96	4.32	3.42	1.74	1.72
18	4.27	4.47	3.70	4.04	4.22	4.46	3.63	1.91	1.89
19	4.36	4.51	3.61	4.16	4.29	4.40	3.76	1.92	1.84
20	4.29	4.61	3.51	4.17	4.35	4.16	3.81	1.76	1.67
21	3.97	4.18	3.58	3.71	3.89	3.58	3.34	1.81	1.71
22	3.37	3.85	3.34	3.24	3.80	3.34	3.25	1.47	1.47
23	2.36	2.80	2.30	2.62	2.77	2.50	2.33	1.26	1.26
24	1.65	1.77	2.19	1.54	1.79	1.62	1.48	0.70	0.68

Table 5-8: Incident short wave (<28.5 s) results for the development layout at the inside points (see Figure 5-11 for locations of the points and Table 5-1 for the cases).

Inside Point	Incident Short Wave H_{m0} (<28.5 s) [m]								
	Case 8	Case 10	Case 16	Case 24	Case 20	Case 20.1	Case 22	Case 26	Case 27
1	2.43	2.78	2.31	2.53	2.71	2.70	2.41	1.51	1.49
2	1.98	2.19	1.96	2.04	2.11	2.14	1.91	1.32	1.27
3	1.44	1.57	1.47	1.47	1.51	1.42	1.30	0.80	0.78
4	1.00	1.06	1.01	0.96	0.98	0.90	0.79	0.60	0.55
5	0.84	0.81	0.50	0.92	0.76	0.66	0.72	0.60	0.50
6	0.96	0.94	0.59	0.99	0.91	0.76	0.89	0.43	0.43
7	1.05	1.11	0.68	1.18	1.12	1.03	1.05	0.76	0.75
8	0.90	0.97	0.82	1.11	0.97	1.00	0.94	0.92	0.85
9	0.55	0.41	1.04	0.52	0.39	0.33	0.38	0.30	0.21
10	0.65	0.61	0.52	0.78	0.59	0.51	0.59	0.35	0.31
11	0.76	0.72	0.55	1.03	0.71	0.60	0.79	0.63	0.55
12	0.75	0.70	0.57	1.00	0.69	0.60	0.80	0.60	0.52
13	1.13	1.08	0.85	1.47	1.01	0.83	1.23	0.80	0.69
14	0.97	0.95	0.64	1.14	0.87	0.77	1.00	0.53	0.51
15	1.04	1.07	0.77	1.10	0.98	0.93	0.86	0.73	0.67
16	1.03	1.14	0.93	1.17	1.12	1.10	0.94	0.84	0.80
17	1.58	1.77	1.69	1.85	1.78	1.72	1.57	1.13	1.15
18	1.25	1.33	1.12	1.30	1.28	1.10	1.12	0.52	0.53
19	1.39	1.50	1.52	1.42	1.43	1.27	1.25	0.67	0.64
20	1.85	2.04	1.80	2.32	2.00	1.77	1.97	1.22	1.14
21	1.70	1.82	1.48	1.85	1.72	1.47	1.58	0.83	0.77
22	1.78	1.86	1.72	1.82	1.72	1.51	1.51	0.77	0.68
23	2.16	2.20	1.89	2.10	2.05	1.76	1.75	0.91	0.79
24	2.39	2.45	2.00	2.28	2.24	1.94	1.87	0.90	0.81
25	2.34	2.42	1.92	2.21	2.19	1.93	1.88	0.80	0.76
26	2.48	2.53	1.77	2.31	2.33	2.04	2.02	0.88	0.82
27	2.57	2.60	1.82	2.34	2.42	2.14	2.10	0.98	0.92
28	2.18	2.19	1.71	1.95	2.06	1.81	1.81	0.74	0.69
29	2.00	2.01	1.40	1.76	1.93	1.65	1.71	0.73	0.68
30	1.94	1.98	1.19	1.72	1.90	1.67	1.66	0.82	0.77
31	1.53	1.59	0.83	1.38	1.53	1.35	1.34	0.53	0.49
32	1.44	1.44	0.78	1.47	1.40	1.21	1.37	0.57	0.49
33	1.24	1.19	0.60	1.36	1.17	0.98	1.24	0.62	0.51
34	0.96	0.90	0.77	0.91	0.86	0.77	0.81	0.39	0.32
35	1.08	1.06	1.15	0.94	0.99	1.04	0.77	0.49	0.41
36	1.49	1.61	1.37	1.80	1.60	1.65	1.48	1.05	0.91
37	1.82	2.04	1.30	2.08	2.04	1.98	1.82	1.16	1.07
38	2.87	2.90	1.83	2.78	2.86	2.44	2.77	1.10	1.04
39	2.35	2.53	1.35	2.61	2.55	2.21	2.47	1.17	1.06
40	3.30	3.11	2.37	2.78	3.01	2.74	2.71	1.24	1.18

Figure 5-16 presents a timeseries of surface elevation extracted at Points 11, 25 and 34 inside the development for Case 10.

Figure 5-16: Timeseries of surface elevation inside the development at Points 11, 25, and 34, 475-year candidate (Case 10). H_{m0} = 9.03 m, T_p = 15 s, Dir = 287.5°, SWL = 2.15 m MSL, SLR for 2074.

The plot shows that the short waves are relatively small along the sheltered edges of the development (Points 11 and 34) and there is a much longer wave that dominates the surface elevations. The timeseries at Point 25 shows that the short waves drive the surface elevations opposite the entrance to the bay.

5.4.4 Overtopping inside the proposed development

Table 5-9 presents the average overtopping discharge rates for the 15 sections along the crest of the new development, while the results are presented visually in Figure 5-17, which also presents overtopping limits for pedestrians and vehicles obtained from EurOtop (2018). Only the cases modelled with the structure were included in Table 5-9 and of those only the cases where some overtopping occurred are included in Figure 5-17.

Table 5-9: Average overtopping discharges for the 15 sections (see Figure 5-12) along the development.

Discharge	Average Overtopping Discharge [l/s/m]								
	Case 8	Case 10	Case 16	Case 20	Case 20.1	Case 22	Case 24	Case 26	Case 27
BW01	27.6	41.9	6.6	32.8	24.7	6.3	2.8	0.0	0.0
BW02	6.8	2.6	3.1	4.5	2.2	0.2	0.0	0.0	0.0
BW03	7.7	5.1	0.1	6.0	0.1	0.0	0.0	0.0	0.0
BW04	4.1	2.0	0.0	0.7	0.0	0.0	0.0	0.0	0.0
BW05	0.0	0.0	0.0	0.0	0.0	0.0	0.0	0.0	0.0
BW06	0.0	0.5	0.0	0.5	0.0	0.0	0.0	0.0	0.0
BW07	11.8	11.3	0.7	5.8	0.9	0.0	0.0	0.0	0.0
BW08	20.7	18.2	2.2	12.6	3.0	1.3	1.7	0.0	0.0
BW09	36.2	31.3	2.7	21.5	8.1	4.4	3.1	0.0	0.0
BW10	15.1	11.1	0.5	7.5	2.0	0.9	0.4	0.0	0.0
BW11	24.2	12.0	0.0	3.0	0.3	0.0	0.0	0.0	0.0
BW12	31.0	11.5	0.0	3.6	0.3	0.0	0.0	0.0	0.0
BW13	8.6	6.2	0.0	3.2	1.2	0.0	0.0	0.0	0.0
BW14	67.5	54.0	1.8	36.0	19.2	2.4	1.8	0.0	0.0
BW15	84.0	83.5	7.7	59.7	40.3	8.2	8.1	0.0	0.0

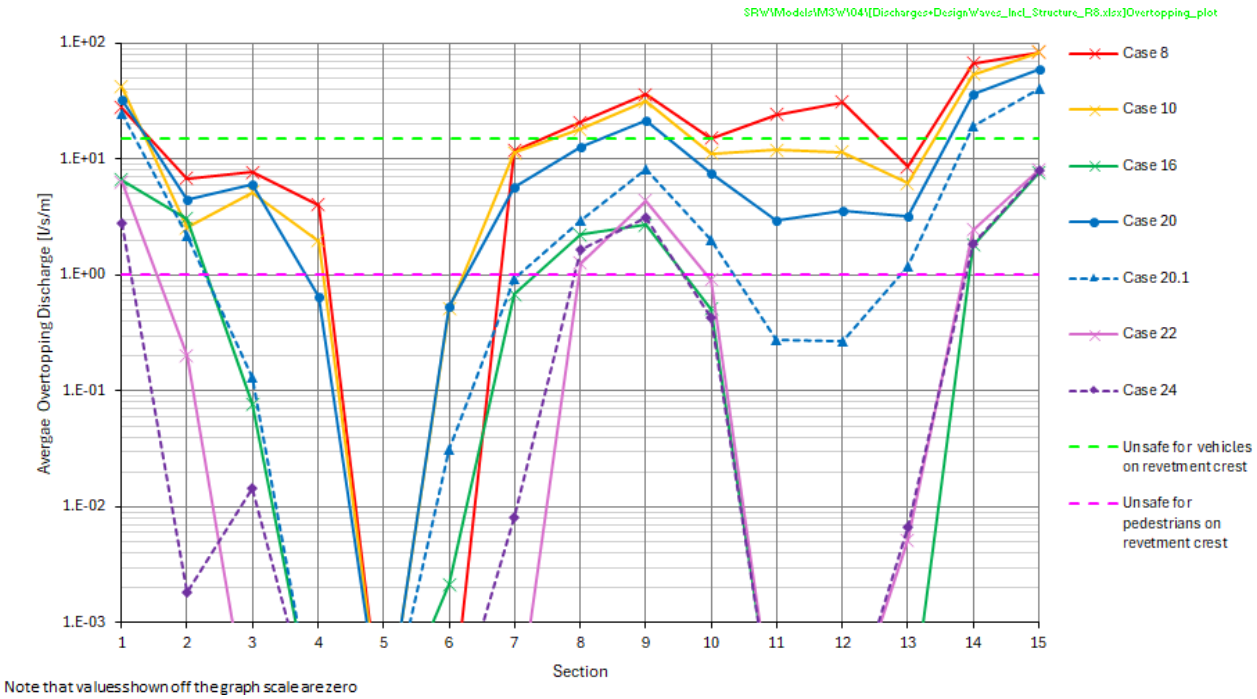

Figure 5-17: Average overtopping discharge for the 15 sections for modelled cases where overtopping of the structure occurred, and EurOtop (2018) limits for pedestrians and vehicles.

For the 1-month cases (Cases 26 and 27), no overtopping was observed for all the sections. For the 475-year cases, large overtopping occurs over the breakwater and along the inside of the development except at sections 5 and 6.

Figure 5-18 presents the maximum flooding depths on the landside of the development for Case 10.

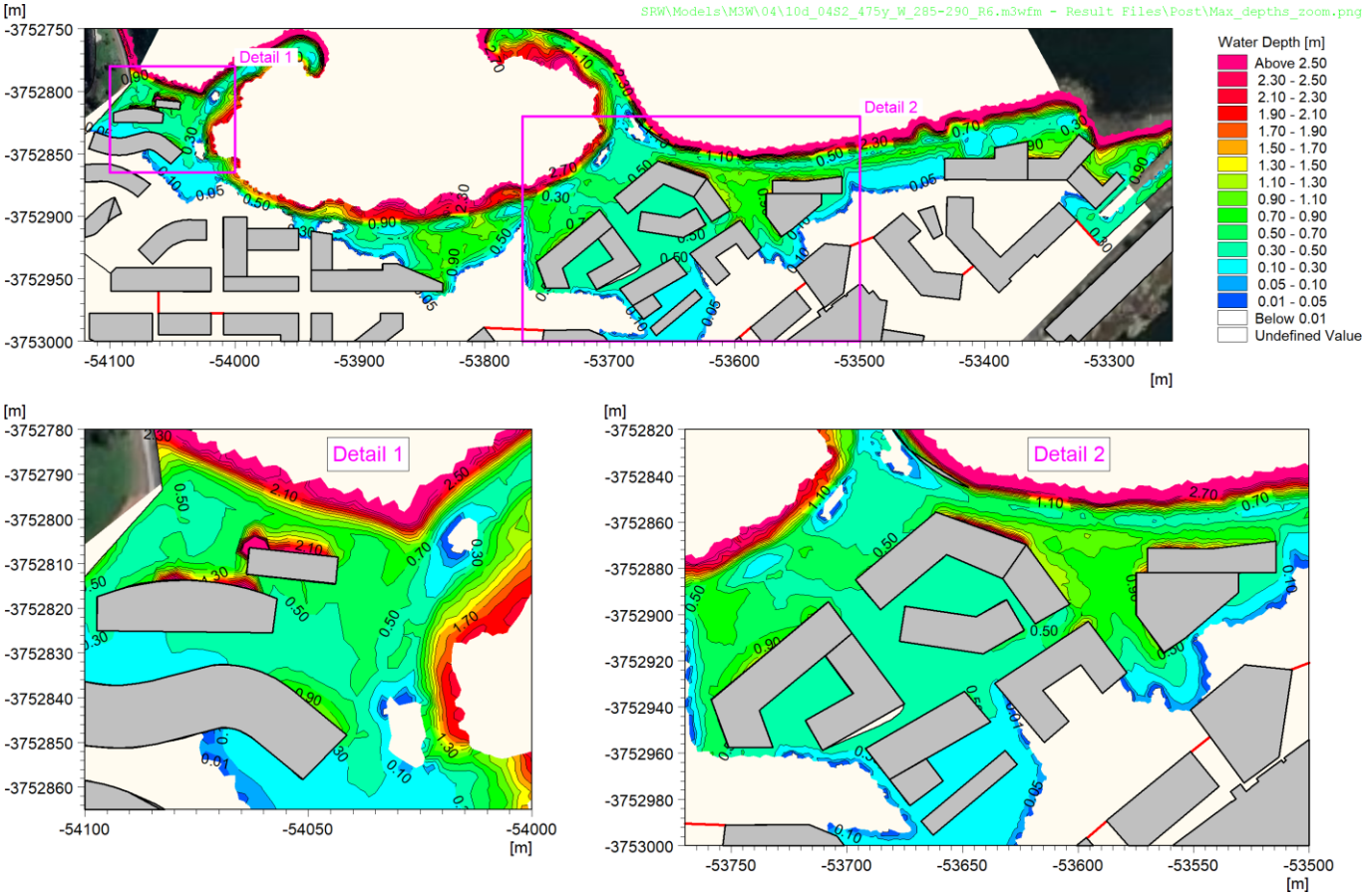

Figure 5-18: Maximum water depth on land for the development layout, 475-year candidate (Case 10). Boundary conditions: H_{m0} = 9.03 m, T_p = 15 s, Dir = 287.5°, SWL = 2.15 m MSL, SLR for 2074.

While these results show some significant flooding depth against structures, it should be noted that the model does not include any landscaping features, storm drains, etc that may significantly alter these results and so they may not be representative of the full development.

Wave conditions were observed to be excessive along the tidal pool located on the inside of the eastern breakwater head, even during the one-month conditions. The height of the tidal pool wall has been raised accordingly.

6. SUMMARY

An assessment of climate change was conducted to determine projections for sea level rise, extreme wave heights and storm surge at Cape Town for two project dates: 2024 (end of construction) and 2074 (end of design life). Long-term water level measurements at Cape Town were analysed to determine extreme storm surge. A calibrated MIKE 21 Spectral Waves model was used to obtain the nearshore extreme wave conditions at the -20 m MSL contour based on 42 years of storms. A joint probability assessment of the extreme waves and storm surge was conducted to determine suitable combinations of extreme waves and water levels.

The MIKE 3 Wave model was used to simulate the processes of key importance, including wave diffraction, wave transmission over the breakwater, wave reflection, and wave-runup and overtopping of edge structures from the -20 m MSL contour to the site of interest. The model was qualitatively validated against observed runup during a historical storm event.

Fourteen cases were modelled in order to provide the various required inputs into the design and the physical model.

The model showed that the short waves are significantly reduced in the lee of the proposed new breakwater, while opposite the entrance between the breakwaters there is less reduction.

Overtopping was determined along the crest edge of the development layout. For the 1-month cases, no overtopping was observed for all the sections. For the 475-year cases, large overtopping occurs over the breakwater and along the inside of the development except at the inner sections south of the western breakwater head.

The results show some significant flooding depths against the landside structures, it should be noted that the model does not include any landscaping features, storm drains, etc that may significantly alter these results and so they may not be representative of the full development.

Wave conditions were observed to be excessive along the tidal pool located on the inside of the eastern breakwater head, even during the one-month conditions. The height of the tidal pool wall has been raised accordingly.

7. REFERENCES

Airshed. (2021). *Proposed methodology for including Climate Change Forecasts into the Duynefontyn Site Safety Report. [CONFIDENTIAL].* Midrand: Airshed Planning Professionals.

DHI. (2024a). *MIKE 21 Toolbox, User Guide.* Hørsholm, Denmark: Danish Hydraulics Institute.

DHI. (2024b). *Extreme Value Analysis, User Guide.* Hørsholm, Denmark: Danish Hydraulics Institute. Retrieved from https://manuals.mikepoweredbydhi.help//2022/General/EVA_UserGuide.pdf

DHI. (2024c). *MIKE21 SW, Spectral Waves FM Module, User Guide.* Copenhagen, Denmark: Danish Hydraulics Institute.

DHI. (2024d). *MIKE 21, Spectral Waves FM Module, Scientific Documentation.* Copenhagen, Denmark: Danish Hydraulics Institute.

DHI. (2024e). *MIKE C-MAP, Extraction of World Wide Bathymetry Data and Tidal Information, User Guide.* Hørsholm, Denmark: Danish Hydraulics Institute.

DHI. (2024f). *MIKE 3, Waves FM Module, User Guide.* Copenhagen, Denmark: Danish Hydraulics Institute.

DHI. (2024g). *MIKE 3, Waves FM Module, Scientific Documentation.* Copenhagen, Denmark: Danish Hydraulics Institute.

DHI. (2024h). *MIKE 3, Wave Model FM. Validation Report.* Copenhagen, Denmark: Danish Hydraulics Institute.

EurOtop. (2018). *Manual on wave overtopping of sea defences and related structures.* EurOtop.

IPCC. (In press). *Climate Change 2021: The Physical Science Basis. Contribution of Working Group I to the Sixth Assessment Report of the Intergovermental Panel on Climate Change.* Cambridge University Press.

Meucci, A., Young, I. R., Hemer, M., Ranashinge, R., & Kirezci, E. (2020). Projected 21st century changes in extreme wind-wave events. *Science Advances*(6), 1-9.

NCEP. (2022). *WAVEWATCH III® Hindcast and Reanalysis Archives*. Retrieved 2022, from https://polar.ncep.noaa.gov/waves/hindcasts/

Petroliagkis, T. I., Voukouvalas, E., Disperati, J., & Bildot, J. (2016). *Joint Probabilities of Storm Surge, Significant Wave Height and River Discharge Components of Coastal Flooding Events. EUR 27824 EN. doi:10.2788/677778.* Italy: European Union.

PRDW. (2021). *Granger Bay Vision. Marine Infrastructure Concept Design Report. S2105-04-RP-CE-001-R0.* Cape Town: PRDW (Pty) Ltd.

PRDW. (2022). *Granger Bay Vision: Wave Modelling Report. S2105-04-RP-CE-002-RA.* PRDW.

Underwater Surveys. (2022). *V&A GRANGER BAY BATHYMETRIC SITE INVESTIGATION.* Cape Town: Underwater Surveys (Pty) Ltd.

PRDW
Consulting Port and Coastal Engineers

For contact or more information, find us at

prdw.com